

Technische Universität Berlin
Fakultät III – Prozesswissenschaften
Institut für Werkstoffwissenschaften und -technologien
Fachgebiet Keramische Werkstoffe

Synthesis and post-processing of COK-12: effect of calcination temperature and freeze-processing of spheres and membranes

Bachelorarbeit

Zur Erlangung des akademischen Grades Bachelor Science (B. Sc.) of
Chemieingenieurwesen

vorgelegt von

Diego Díaz Cubas

Geboren am: 13.05.1995

in: Valencia

Matrikelnummer: 389024

Berichter: Prof. Dr.-Ing. Aleksander Gurlo

Mitberichter: Maria Gracia Colmenares und Ulla Simon

Tag der Einreichung 02. Oktober 2017

Acknowledgements

I would like to express my deepest gratitude to those who contributed to the completion of my thesis.

First of all to Prof. Dr. Aleksander Gurlo and my two tutors, María Colmenares and Ulla Simon. This thesis would have been imposible without them.

Also to other people of the ceramics deparment: Oliver, Maged, Peter, Heinz, Harald, Kai, Albert, Xifan and Anne-Claude. Thank you all so much for helping me always when I needed something and teaching me so many things.

Abstract

Ordered mesoporous silica materials, also called OMS, are a groups of silica nanomaterials with ordered pores, which size can be from 2 to 50 nm. They have been used a lot since 1990 in several fields such as drug delivery, adsorption, separation and catalysis. The most widely known OMS is SBA-15, but COK-12, wich was discovered in 2010, has analogous properties and it's synthesis shows some advantages in comparison to SBA-15. COK-12 synthesis takes place at room temperature and almost neutral pH and it's quicker, more inexpensive and environmetally friendly.

In this thesis two different synthesis methods of the ordered mesoporous silica material COK-12 were studied, in order to find the best synthesis method according to the properties requirements in each case. In each of both synthesis methods there were some variations in the process and the changing properties of the final product were studied, specially the pore morfology and the surface characteristics.

As COK-12 has applications in catalysis and adsorption, spheres and membranes with COK-12 in different compositions were produced in this work. The results are shown in this thesis.

Kurzfassung

Ordered Mesoporous Silica Materialien, auch OMS genannt, sind eine Gruppe von Siliciumdioxid-Nanomaterialien mit geordneten Poren, deren Größe von 2 bis 50 nm liegen kann. Sie wurden seit 1990 in mehreren Bereichen wie Drogenabgabe, Adsorption, Trennung und Katalyse verwendet. Das bekannteste OMS ist SBA-15, aber COK-12, das 2010 entdeckt wurde, hat analoge Eigenschaften und seine Synthese zeigt einige Vorteile im Vergleich zu SBA-15. Die COK-12-Synthese erfolgt bei Raumtemperatur und nahezu neutralem pH-Wert und ist schneller, preiswerter und umweltfreundlicher.

In dieser Arbeit wurden zwei verschiedene Synthesemethoden des geordneten mesoporösen Siliciumdioxidmaterials COK-12 untersucht, um das beste Syntheseverfahren nach den jeweiligen Eigenschaftsanforderungen zu vervollständigen. Bei jedem der beiden Synthesemethoden gab es einige Variationen in dem Verfahren und die sich ändernden Eigenschaften des Endprodukts wurden untersucht, insbesondere die Porenmorphologie und die Oberflächeneigenschaften.

Da COK-12 Anwendungen in der Katalyse und Adsorption hat, wurden in dieser Arbeit Sphären und Membranen mit COK-12 in verschiedenen Zusammensetzungen hergestellt. Die Ergebnisse werden in dieser Arbeit gezeigt.

Table of contents

Acknowledgements.....	i
Abstract.....	ii
Kurzfassung	iii
Introduction	vi
1. Literature review.....	1
1.1 General considerations on porous solids.....	1
1.2 Ordered mesoporous silica materials.....	2
1.3 Synthesis of ordered mesoporous silica.....	2
1.3.1 Synthesis mechanism	2
1.3.2 Synthesis of COK-12.....	4
1.4 Sphere production	5
1.5 Film production.....	5
2. Characterization methods	6
2.1 Small-angle X-ray diffraction	6
2.2 Nitrogen sorption	7
2.3 Scanning electron microscopy.....	10
2.4 Energy-dispersive X-rayspectroscopy.....	11
2.5 Transmission electron microscopy.....	11
2.6 Infrared Spectroscopy.....	11
2.7 Inductively Coupled Plasma-Optical Emission Spectroscopy	12
2.8 Elemental Analysis.....	13
3. Experimental.....	14
3.1 COK-12 batch synthesis.....	14
3.1.1 Reference material synthesis: powder COK-12	14
3.2 Extraction and calcination temperature.....	16
3.3 Spheres production.....	18
3.3.1 Solubility test	20
3.3.2 Water purification test	21
3.4 Tape production	22
4. Results and discussion	24
4.1 Influence of calcination temperature on pore morphology and surface characteristics.....	24
4.2 Influence of extraction on pore morphology and surface characteristics	35

4.3	Spheres.....	38
4.3.1	Spheres analysis	38
4.3.2	Solubility test.....	52
4.3.3	Water purification test	52
4.4	Tape production.....	55
5	Conclusions and outlook	59
6	References	60
	List of figures	62
	List of tables	64

Introduction

Ordered mesoporous silica materials (OMS) have very interesting properties, such as controlled size ordered pores fewer than 20 nm wide and large surface areas. They have many application fields, for example, catalysis or drug delivery.

A relatively new OMS material, the COK-12, could be used a lot in the future, because it has analogous properties to another OMS material which is being used nowadays, the SBA-15. But the synthesis of COK-12 takes place at room temperature and almost neutral pH and it's much more environmentally friendly. The fact that COK-12 is formatted almost immediately could theoretically permit it's continuous synthesis.

The first part of this thesis is about the synthesis and batch upscaling of COK-12. The material produced has been later used for investigation, which is also reported in this thesis. In this part, the first purpose is to produce COK-12 in large quantities, maintaining its characteristic mesostructure.

The second part of this thesis consist of a calcination temperature study in order to see how the COK-12 and its pores change. As the calcination temperature used in the synthesis according to Jammaer, et. al.¹ is 500°C, calcination temperatures between 350°C and 900°C have been studied. In this part, another method of elimination of P123 was studied. In stead of calcining the copolymer, it was extracted with methanol, which is cheaper, quicker and with less environmental impact. Keeping in mind that the properties of COK-12 change with different calcination temperatures, the second purpose of this work is to report about the material characteristics at each calcination temperature, trying to find the optimum depending on the properties needed for each application.

The third part of this work deals with the production of spheres of alginate and COK-12. Two methods were used: production with liquid nitrogen and production with calcium chloride. Using the COK-12 produced in batch, spheres of diverse compositions were produced and later analyzed in order to characterize them. The third purpose is to use the COK-12 in form of spheres, which is interesting for some applications like wáter purification.

The fourth part of this thesis comprises the production of membranes or films compound of alginate and COK-12. For its production, tape casting was used, freezing the solution almost immediately with liquid nitrogen and later drying it in the freeze dryer. The last purpose of this work is to produce membranes with COK-12 inside, which could be interesting for applications such as catalysis.

This thesis is organized as follows:

Chapter 1 includes a historical overview of OMS materials, the synthesis mechanism of them and the synthesis of COK-12.

Chapter 2 presents the characterization methods used throughout this work.

Chapter 3 includes the synthesis and upscaling of COK-12 with the different calcination temperatures and the extraction with methanol as an alternative to calcination. It also describes the production of spheres and films.

Chapter 4 presents the results of the thesis, discussing the calcination temperatures, the methanol extraction and the characterization of spheres and films.

Chapter 5 summarizes the main results of this study and highlights future perspectives for this work.

1. Literature review

1.1 General considerations on porous solids

There are many materials that contain pores, which are usually filled with a liquid or gas. The skeletal material can be a solid or a foam. A porous solid is a solid that contains cavities, channels or interstices which are deeper than they are wide. These cavities, or pores, are classified as described in Table 1.1².

The porosity of a material is given in a percentage and it is a fraction of the volume of voids over the total volume. Porosity is used in multiple fields, such as ceramics, metallurgy or engineering.

Table 1.1 Classification of pores according to the IUPAC.

Classification according to	Type of pores	Description
Size:	Microporous	<2 nm
	Mesoporous	2-50 nm
	Macroporous	>50 nm
Availability to an external fluid:	Closed pores	Completely isolated pores (Figure 1.1 a)
	Open pores	Continuous channel of communication with external surface (Figure 1.1 b, c, d, e, f)
	Blind pores	Open on one end (Figure 1.1 b,f)
	Through pores	Open on two ends (Figure 1.1 e)
Shape:	Cylindrical	Either open (Figure 1.1 c) or blind (Figure 1.1 f)
	Ink-bottle	Figure 1.1 b
	Funnel-shaped	Figure 1.1 d
	Slit-shaped	Figure 1.1 c

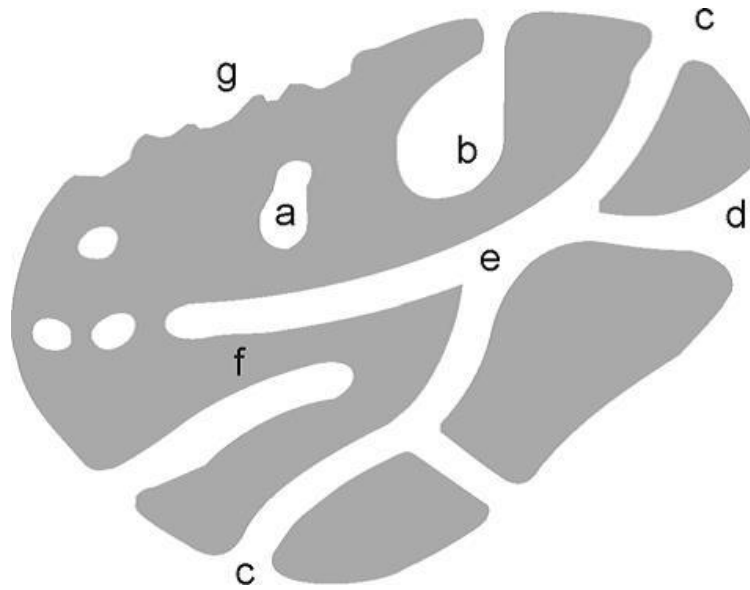


Figure 1.1 Illustrative cross-section of a porous solid². For details see Table 1.1

1.2 Ordered mesoporous silica materials

Ordered mesoporous silica (OMS) materials were discovered in the early 1990s and have become of interest for their special properties. OMS materials belong to the family of silica nanomaterials and they have a structure of solid silica with ordered and equally distributed pores. Those pores can be between 2 and 50 nm wide.

Ordered mesoporous materials have many application areas, such as drug delivery³, electrochemistry⁴, sensing⁵, diadsorption⁶, separation⁷ and catalysis⁸.

1.3 Synthesis of ordered mesoporous silica

1.3.1 Synthesis mechanism

Ordered mesoporous silica materials can be synthesized by two different templating methods: *soft-templating*, which is based on a co-assembly of silica and surfactant molecules or *hard-templating*, in which the structure-directing agent is a structured solid.

There are different mechanisms for the softtemplating of OMS. The first mechanism is called *true liquid crystal templating* mechanism, in which a high concentration of the templating surfactant leads to the formation of mesophases prior to the addition of silica. The second mechanism is the *cooperative self-assembly* mechanism, where the process of self-assembly occurs even at low surfactant concentrations guided by the interactions between surfactant and silica⁹.

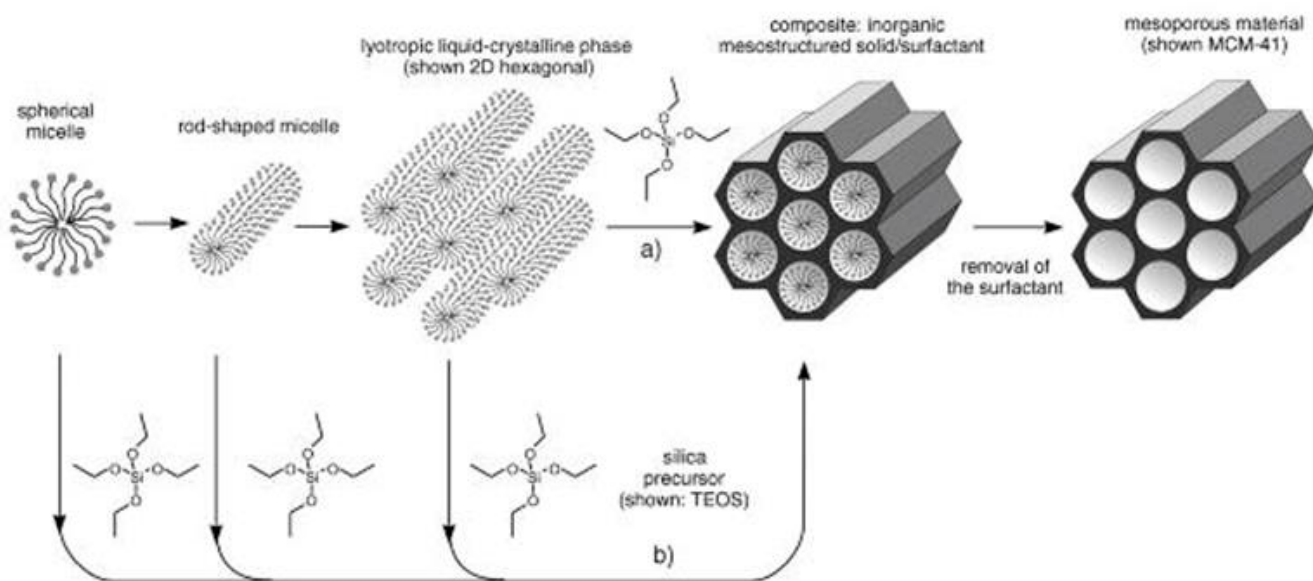


Figure 1.2 True liquid crystal templating mechanism (a) and the cooperative self-assembly mechanism (b) for production of MCM-41¹⁷.

Cooperative self-assembly

1.3.1.1 Processes involved in ordered mesoporous silica synthesis

In this work, the OMS has been synthesized following the precipitation protocol, which consists of five steps: reaction, solid recovery, washing, drying and template removal.

The first step consists of two sub-steps: reaction and maturation. In the first sub-step, reactants are mixed, they react and the solid phase precipitates. This precipitation can take more or less time depending on the synthesis parameters. The maturation or aging sub-step is often required to consolidate the silica walls by increasing the degree of condensation. In this step temperatures up to 150 °C and maturation times up to 48 h can be required.

In the second step, solid recovery, vacuum filtration is usually used to separate the solid organic-inorganic hybrid from the solvent. This step could be a difficulty in the continuous OMS synthesis.

In the third step, washing, the recovered solid is washed in order to remove by-products and other unwanted components. It can have an influence on the final properties of the material and it is also useful, because it can help in the removal of the templating agent, reducing the amount of energy that needed in the final step.

The fourth step, drying, takes place at temperatures between 50 and 80 °C and it can produce some changes in the mesophase structure depending on the initial reaction conditions. Therefore, the reaction time and the drying temperature should be controlled to obtain the wished properties for the final material.

The most common method of template removal, which is the last step, is calcination and in some cases extraction is also used. Calcination temperature has to be chosen depending on the molecule used as a template. Higher calcinations temperatures imply that the template will be completely removed, but it can also modify the properties and the chemical groups in the final mesoporous material. A possibility to avoid it is to use longer calcinations times in stead of higher temperatures. Calcination is more efficient than extraction, but with calcination the template gets destroyed and can not be reused.

1.3.2 Synthesis of COK-12

COK-12 is produced in a faster, inexpensive and more environmentally-friendly way in comparison to other OMS materials. It is synthesized at room temperature by incorporating a solution of sodium silicate to a buffered (pH = 4-5) aqueous solution of spherical P123 micelles. Details are explained in section 3.1.1.

The stages of formation of COK-12 can be observed in Figure 1.3, where there is a short explanation of each step.

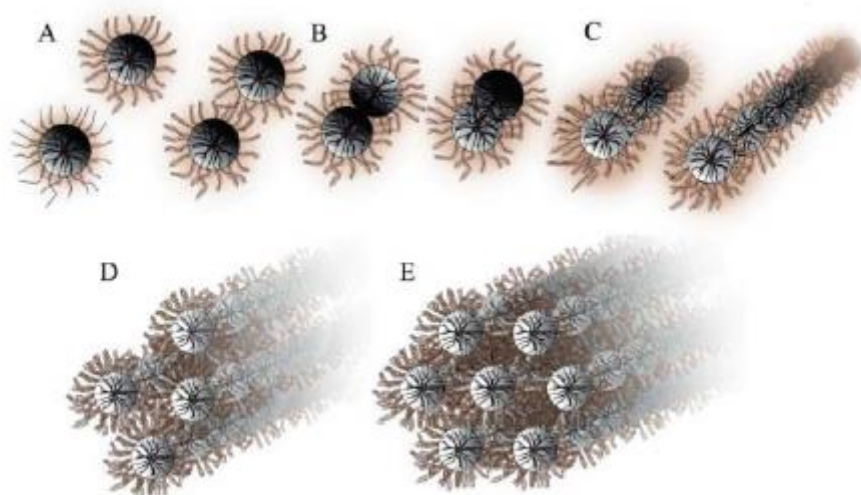


Figure 1.3 Schematic representation of the stages of formation of COK-12. (a) Silica species precipitate on the PEO blocks of the spherical P123 micelles which are in solution. (b) At a critical silica concentration, steric stabilization is lifted and (c, d) spherical micelles coalesce into cylinders that increase in size. (e) Further addition of silica species leads to the aggregation of the cylinders and eventually to the formation of a 2-dimensional hexagonally ordered mesostructure¹¹.

1.4 Sphere production

Spheres is a very useful shape for some materials for further applications, like water purification, where it is easier to remove the material if it is in form of spheres. Therefore, spheres consisting partially of COK-12 have been studied during this work. There are several ways to produce spheres and in this work the spheres have been produced by dropping the different solutions into liquid nitrogen or calcium chloride solutions, so that the spheres have been formed immediately by shaping and solidification. The concrete procedure is explained in the experimental part of the thesis.

1.5 Film production

As COK-12 has many application areas, there are some of them where it could be interesting to have the OMS material in form of a film or membrane. Separation and catalysis are two examples where it could be useful to have a film containing COK-12. To produce the films of the different compositions, a freezing process with liquid nitrogen was used. The method is explained in detail in the experimental part.

2. Characterization methods

In this section, the characterization techniques used to characterize the materials produced are described. There is an overview of the technique, the information that can be obtained with each technique and methods for sample preparation. Characterization of COK-12 materials and its granules includes:

- Small-angle X-ray diffraction: pore ordering analysis
- Nitrogen sorption: pore shape analysis, determination of specific surface area, pore volume and pore size distribution
- Transmission electron microscopy: pore size, shape and ordering analysis.
- Scanning electron microscopy: morphological analysis
- Infrared spectroscopy: analysis of chemical composition
- Energy-dispersive X-ray spectroscopy: elemental surface analysis
- Inductively coupled plasma optical emission spectroscopy: analysis of impurities
- Elemental analysis

2.1 Small-angle X-ray diffraction

Small-angle X-ray diffraction (SAXS) is used for the determination of the microscale or nanoscale structure of particle systems in terms of such parameters as averaged pore sizes, shapes, distribution, and surface-to-volume ratio. It's a non-destructive and accurate method and it usually requires only a minimum of sample preparation. For structural crystallographic analysis on an atomic level, large 2θ values are used. Using small 2θ values (usually between 0.1° to 10°), domains with larger dimensions can be studied, between 1 and 200 nm (small-angle X-ray diffraction, SAXRD). With SAXRD it is possible to determine the lattice parameter a , which corresponds to the distance between the center of each pore, and the interplanar spacing d for a given orientation.

Given their wavelength, X-rays can penetrate bulk solids and interact with matter, giving information regarding the crystallographic or structural properties of the material. By measuring the angle-dependent distribution of scattered radiation (intensity), it is possible to draw conclusions about the average particle structure².

Given that the radiation waves emitted by neighboring atoms are synchronized, coherent waves are produced that result in constructive interference, which gives information about the particle structure that depends on the angle of observation 2θ . This scattering of waves in specific directions is represented by Bragg's law:

$$2d_{hkl} \sin \theta_{hkl} = n\lambda$$

Where:

d: interplanar distance of the hkl planes

θ : scattering angle of the hkl planes

n: positive integer naming the order of the reflection
 λ : wavelength of the incident wave

The scattering planes are recognized by the Miller indices (hkl).

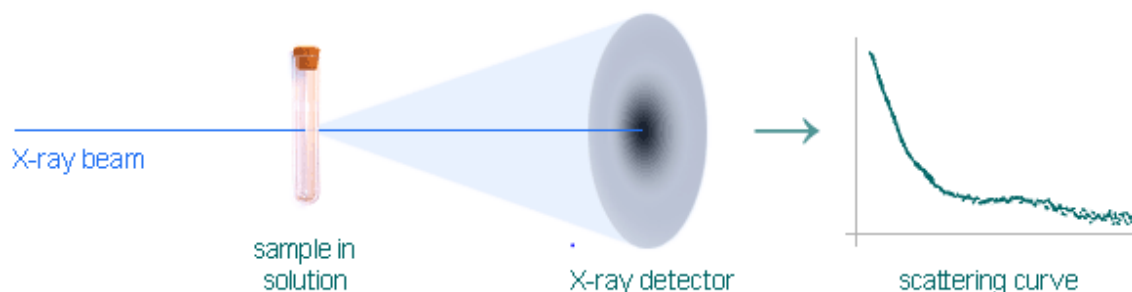


Figure 2.1 Schematic representation of the functioning of SAXS¹⁸.

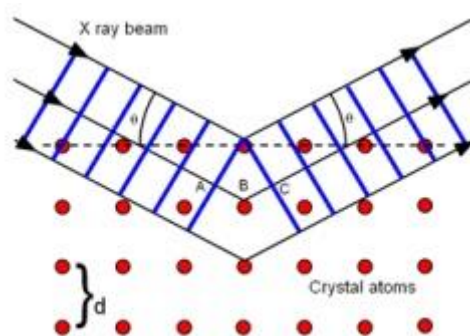


Figure 2.2 Bragg's law of diffraction, in which three radiation waves of identical wavelength interact with three atoms within crystalline solid and are scattered¹⁹.

For this work, small-angle X-ray diffraction curves were obtained using a Bruker AXS D8 ADVANCE X-ray diffractometer with a Bragg–Brentano geometry equipped with a Lynx Eye 1D detector (CuK α 1 radiation wavelength 0.15406 nm). Measurements were carried out between 0.5 and 6.0° 2 θ value, with a step time of 1 s/0.0003° at 35 kV and 40 mA and with a 280 mm sample-detector distance. The patterns were analyzed using the Diffrac-Plus/EVA software from Bruker AXS, reflections were identified using the same software.

2.2 Nitrogen sorption

The adsorption of nitrogen is a method used to determine the specific surface area of porous materials. The relation between the amount adsorbed and the equilibrium pressure of nitrogen is known as the *adsorption isotherm*. Depending on the size and shape of the pores, the physisorption behavior varies.

Physisorption can be divided in two cases: In the case of pores less than 2nm wide (*micropore filling*), physisorption occurs in one single step. In the case of pores between 2 and 50 nm wide (mesopores), physisorption is a two-step process, called *monolayer-multilayer adsorption* and *capillary condensation*².

When all the adsorbed molecules are in contact with the surface layer of the adsorbent, monolayer adsorption occurs. In multilayer adsorption, by increasing the pressure, the adsorption space accommodates more than one layer of molecules. Next step after monolayer-multilayer adsorption is the capillary condensation, which occurs below the pure liquid's saturation pressure. During this step the remaining available pore space is filled with condensate that is separated from the gas by a meniscus. This process differs from micropore filling in the fact that there is no meniscus formation in the latter².

Sorption data is presented graphically in the form of adsorption isotherms, plotting the amount adsorbed against the equilibrium relative pressure. The International Union of Pure and Applied Chemistry (IUPAC) has established an adsorption isotherms classification. (Figure 2.3)

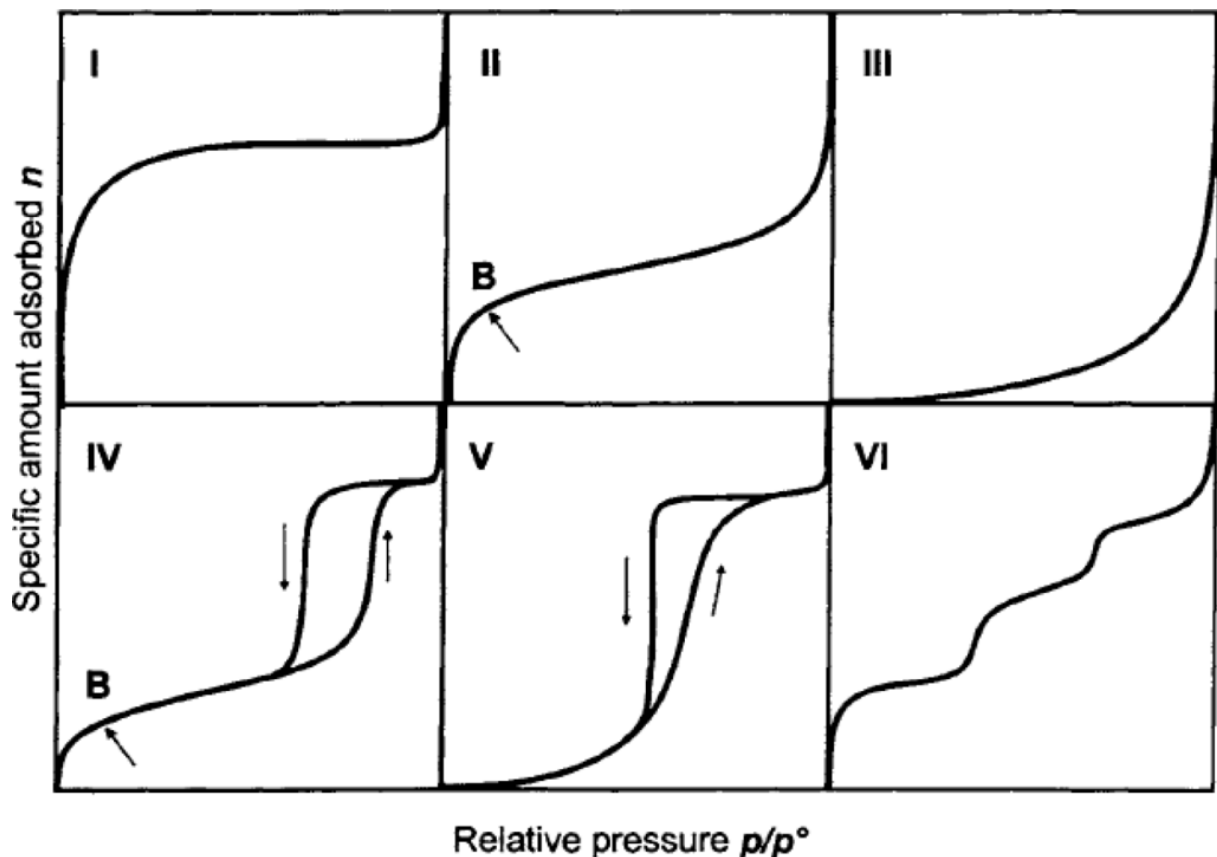


Figure 2.3 Types of adsorption isotherms as classified by IUPAC². See text for details.

Type I isotherm result from microporous solids with relatively small external surface.

Type II isotherm is obtained with a non-porous or macroporous adsorbent, in this type of isotherm the point *B* indicates the stage at which monolayer coverage is complete and multilayer adsorption begins.

Type III isotherms occur when there is a weak interaction between the adsorbate and adsorbent.

Type IV isotherms exhibit a characteristic hysteresis loop, which is associated to capillary condensation, and also exhibits the initial monolayer-multilayer adsorption behavior. This type of isotherm is very common for many industrial adsorbents.

Type V isotherm is uncommon, and is also related to weak adsorbate-adsorbent interaction. Type VI isotherm represents stepwise multilayer adsorption on a uniform nonporous surface.

Looking at the hysteresis in adsorption isotherms, information can be obtained. First, monolayer adsorption occurs (Figure 2.4 A, B, C). The next step, capillary condensation, takes place by increasing the pressure at a critical adsorbed film thickness, so that the adsorbed volume increases and it is associated with the pore dimensions (Figure 2.4 C, D). At the beginning of desorption, evaporation occurs at lower relative pressures than condensation, so that the hysteresis loop is formed (Figure 2.4 E, F). It is related to the pore opening.

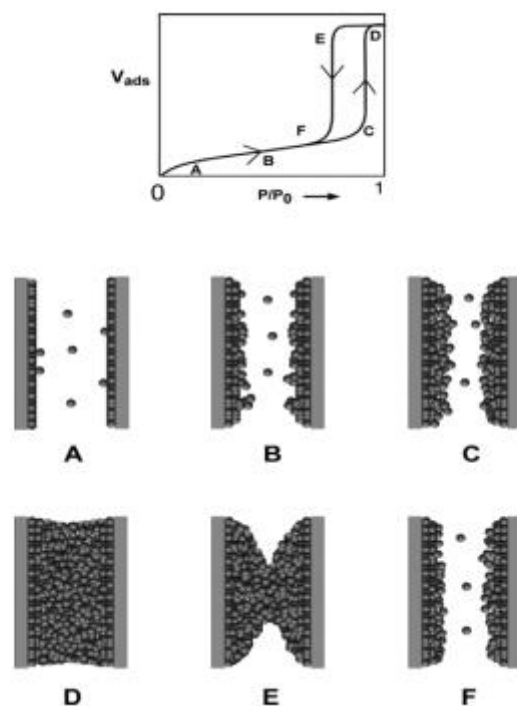


Figure 2.4 Schematic representation of multilayer adsorption, pore condensation and hysteresis in a single pore. (A) monolayer formation, (B) multilayer adsorption, (C-D) capillary condensation, (E) pore evaporation by a receding meniscus, (F) desorption²⁰.

In Figure 2.5, four types of hysteresis can be seen. In hysteresis type H1, often associated with mesoporous materials with uniform pore size and cylindrical, the two branches are almost vertical and parallel over a large adsorbed volume range. It can be associated with mesoporous materials with uniform pore size and cylindrical pores. Type H2 hysteresis is often associated with spherical pores with narrow openings that connect them. Type H3 hysteresis is associated with aggregates of plate-like particles that give rise to slit-like pores. In type H4, associated with narrow slit-like pores, the branches are nearly horizontal and parallel.

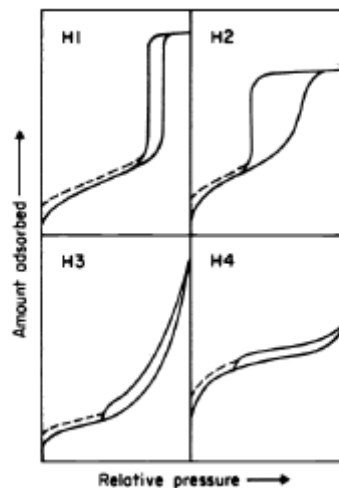


Figure 2.5 Types of hysteresis loops as classified by IUPAC².

Nitrogen sorption isotherms were recorded at 77 K on a Quadra Sorb Station 4 apparatus after degassing for 10 h at 200 °C under vacuum. Surface area was determined using the BET method. Although the BJH method is widely accepted for the estimation of pore size distribution for cylindrical pores, it can underestimate the size when pores are smaller than 5 nm in diameter. For this reason, the pore size distribution determination of cylindrical mesopores was based on nonlocal density functional theory (NLDFT). Pore size distribution of micropores was based on t-plot methods. All data was analyzed using the Quantachrome/QuadraWin software.

2.3 Scanning electron microscopy

A scanning electron microscope (SEM) scans a focused electron beam over a surface to create high-resolution images. The electrons in the beam interact with the sample, producing various signals that can be used to obtain information about the surface topography and composition. SEM imaging is used in this work to study the morphology of the synthesized materials, specially in the case of the spheres and films.

Imaging was carried out on a Zeiss Gemini Leo 1530 with integrated energy-dispersive X-ray spectroscopy (Noran System 6, Thermo Scientific). Samples were immobilized on conducting carbon pads and then sputtered with a thin layer of gold to prevent charging. Some samples were immobilized in epoxy resin and sanded with 180 grit sanding paper.

2.4 Energy-dispersive X-rayspectroscopy

Energy-dispersive X-ray spectroscopy (EDX) is an analytical technique used for the elemental analysis or chemical characterization of a sample. The EDS technique detects x-rays emitted from the sample while focusing into the sample an electron beam to characterize the elemental composition of the analyzed compound. When the sample is bombarded by the SEM's electron beam, electrons are ejected from the atoms comprising the sample's surface. The resulting electron vacancies are filled by electrons from a higher state, and an x-ray is emitted to balance the energy difference between the two electrons' states. The x-ray energy is characteristic of the element from which it was emitted.

EDX was carried out on a Zeiss Gemini Leo 1530 scanning electron microscope with integrated energy-dispersive X-ray spectroscopy (Noran System 6, Thermo Scientific). Samples were immobilized on conducting carbon pads and then sputtered with a thin layer of gold to prevent sample charging. Analysis was carried out on the Noran System Six (NSS) software.

2.5 Transmission electron microscopy

The transmission electron microscopy (TEM) operates similar to SEM. However, thin films and small samples are transmitted by an electron beam. TEMs can reveal the finest details of internal structure - in some cases as small as individual atoms. The specimen is most often an ultrathin section less than 100 nm thick or a suspension on a grid. An image is formed from the interaction of the electrons with the sample as the beam is transmitted through the specimen.

A FEI Tecnai G2 20 S-TWIN transmission electron microscope (FEI Company, Eindhoven, Netherlands) equipped with a LaB₆-source at 200 kV acceleration voltage was used. Images were recorded with a GATAN MS794 P CCD-camera. The microstructure (pore size and pore shape/morphology) of the samples was studied at the Department of Electron Microscopy (ZELMI), TU Berlin.

2.6 Infrared Spectroscopy

Infrared spectroscopy (IR) is the analysis of infrared light interacting with a molecule. The IR spectrum of a sample is recorded by passing a beam of infrared light through the sample. This can be analyzed in three ways by measuring absorption, emission and reflection. Molecules absorb frequencies that are characteristic of their structure. Representing the wavenumber in a graph it's possible to analyze the peaks, which are characteristic of specific chemical groups.

IR is used to determine functional groups in molecules. IR Spectroscopy measures the vibrations of atoms, and based on this it is possible to determine the functional groups.

A single atom cannot absorb IR radiation, because it has no bonds. For a symmetric molecule there is no change in dipole when the molecule vibrates, so it will not absorb IR. But for an asymmetric diatomic molecule, the dipole moment will change as the bond stretches or contracts, so HF does absorb IR radiation.

An Agilent Cary 630 FTIR Spectrometer was used and it was measured in attenuated total reflection (ATR).

2.7 Inductively Coupled Plasma-Optical Emission Spectroscopy

Inductively Coupled Plasma-Optical Emission Spectroscopy is a multi-element analytical technique that can provide elemental composition of a wide variety of sample types, such as powders, solids, liquids and suspensions. Solid samples are generally dissolved or digested using a combination of acids in a closed microwave system, thus retaining potentially volatile analyte species. The resulting samples are introduced as aerosol in an argon plasma. The analyte species can then be detected and quantitated with an optical emission spectrometer, which measures the intensity of radiation emitted at the element-specific, characteristic wavelength from thermally excited analyte atoms or ions. Intensity measurements are converted to elemental concentration by comparison with calibration standards.

Inductively coupled plasma optical emission spectroscopy was carried out on a Horiba Scientific ICP Ultima2. Samples were digested in an aqueous suspension with the addition of HNO₃ and HF at 200°C for 5 h in an autoclave.

2.8 Elemental Analysis

Elemental Analysis is a process where a sample of some material (e.g., soil, waste, minerals, chemical compounds) is analyzed for its elemental and sometimes isotopic composition. Elemental analysis can be qualitative (determining what elements are present), and it can be quantitative (determining how much of each are present). Elemental analysis falls within the ambit of analytical chemistry, the set of instruments involved in deciphering the chemical nature of our world.

Elemental analysis was carried out on a Thermo FlashEA 1112 Elemental Analyzer of the Thermo Finnigan Company.

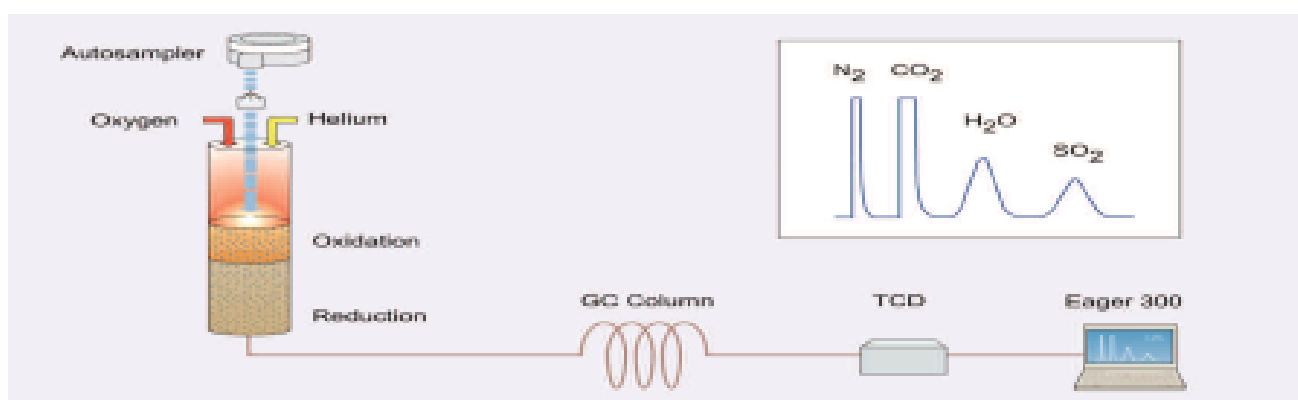


Figure 2.6 Schematic representation of the functioning of elemental analysis²¹.

3. Experimental

3.1 COK-12 batch synthesis

OMS synthesis normally requires harsh synthesis conditions such as very basic or acidic media and high temperature hydrothermal treatments. The discovery of COK-12 marked the first OMS synthesis that circumvents these conditions. The reaction takes place at room temperature and under quasi-neutral pH, and employs a more inexpensive silica source than that used for most OMS materials synthesis¹³. OMS monoliths have found applications in separation¹⁴ and catalysis¹⁵.

3.1.1 Reference material synthesis: powder COK-12

Powder COK-12 was synthesized according to Jammaer, et al.¹⁶, but using 25 times the quantities of the original synthesis protocol.

First of all 100.0 g of the triblock copolymer Pluronic P123 (Sigma-Aldrich) (structure directing agent) were dissolved in 2687.5 ml distilled water (DIW), stirring with a magnetic stirrer. When P123 was totally dissolved, 63.50 g trisodium citrate (Roth) and 92.1 g citric acid monohydrate (Roth) were incorporated to create a buffer with a pH between 4 and 5. After stirring for 24 h, a solution of 260.0 g of sodium silicate (Roth) and 750.0 ml DIW was prepared and added. Solid formation was observed immediately (Figure 3.1). Then the resulting solution was stirred for 5 min and aged for 24 h under static conditions at room temperature. The suspension was then filtered and washed thoroughly with 12500 ml DIW. (Figure 3.1) Solids were dried overnight in a cabinet dryer at 60 °C. After that, two methods to remove the organic templating agent were studied: calcination at different temperatures for 8 h, with a 1°C/min heating ramp or extraction with methanol.

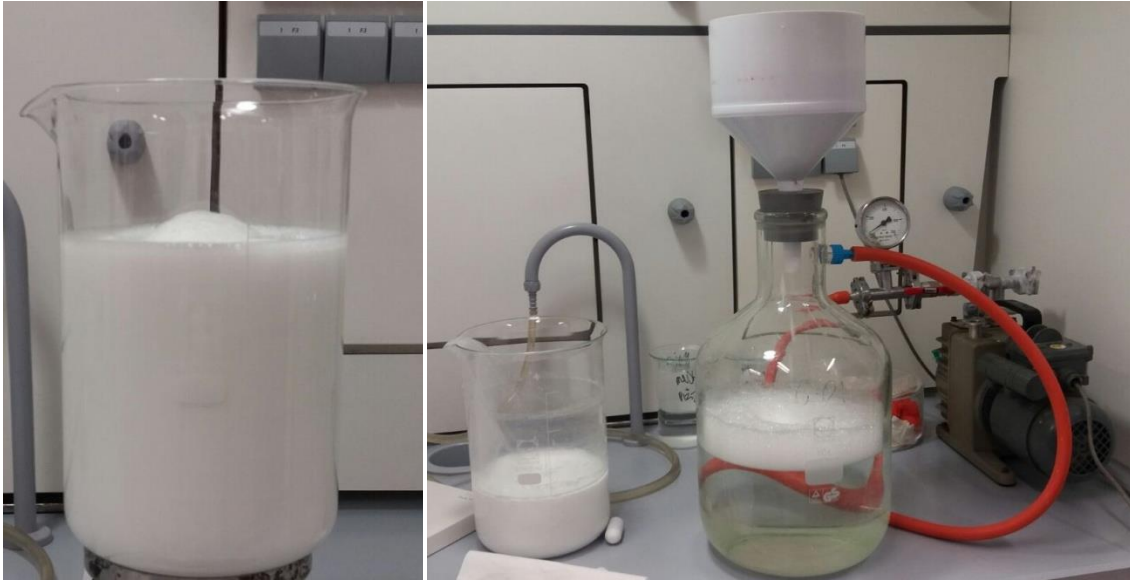


Figure 3.1 Immediately solid formation just after adding the silicate solution (left) and filtration process (right).

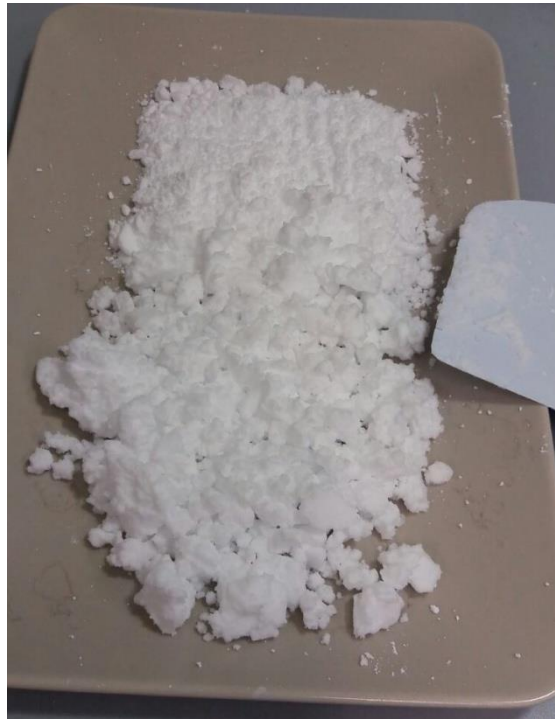


Figure 3.2 Solids after filtration.

Table 3.1 Synthesis conditions for upscaled COK-12 materials synthesis.

Material	Batch size	P123 [g]	DIW ^a [ml]	Citric acid [g]	Sodium citrate [g]	Sodium Silicate [g]	DIW ^b [ml]	DIW ^c [ml]
COK-12-25X	25X	100.0	2687.5	92.1	63.50	260.0	750.0	12500

^aFor P123 solution ^bFor sodium metasilicate solution ^cFor washing

3.2 Extraction and calcination temperature

To study the influence of calcination temperature on pore structure and surface characteristics, calcination was studied at 9 different temperatures ranging between 350 and 900 °C for 8 h and a heating ramp of 1°C/min. (Table 3.3)

Furthermore, instead of calcination the extraction of the soft-template with methanol was investigated. First, 200 ml DIW were added to 2.0 g of the dry uncalcined solid and then it was put in an ultrasonicator at room temperature. After that it was filtered and washed thoroughly with 400 ml methanol. Finally, it was dried overnight in a cabinet dryer at 60°C. Methanol extraction was done varying the time inside of the ultrasonicator. (Table 3.3)

Table 3.2 Calcination temperatures used and times in the ultrasonicator used for the methanol extraction.

Calcination temperature [°C]	Methanol Extraction-time in the ultrasonicator [min]	Sample Code
350		COK-12_350
400		COK-12_450
450		COK-12_400
500		COK-12_500
600		COK-12_600
650		COK-12_650
700		COK-12_700
800		COK-12_800
900		COK-12_900
	10	COK-12_10_MeOH
	2x5	COK-12_2x5_MeOH

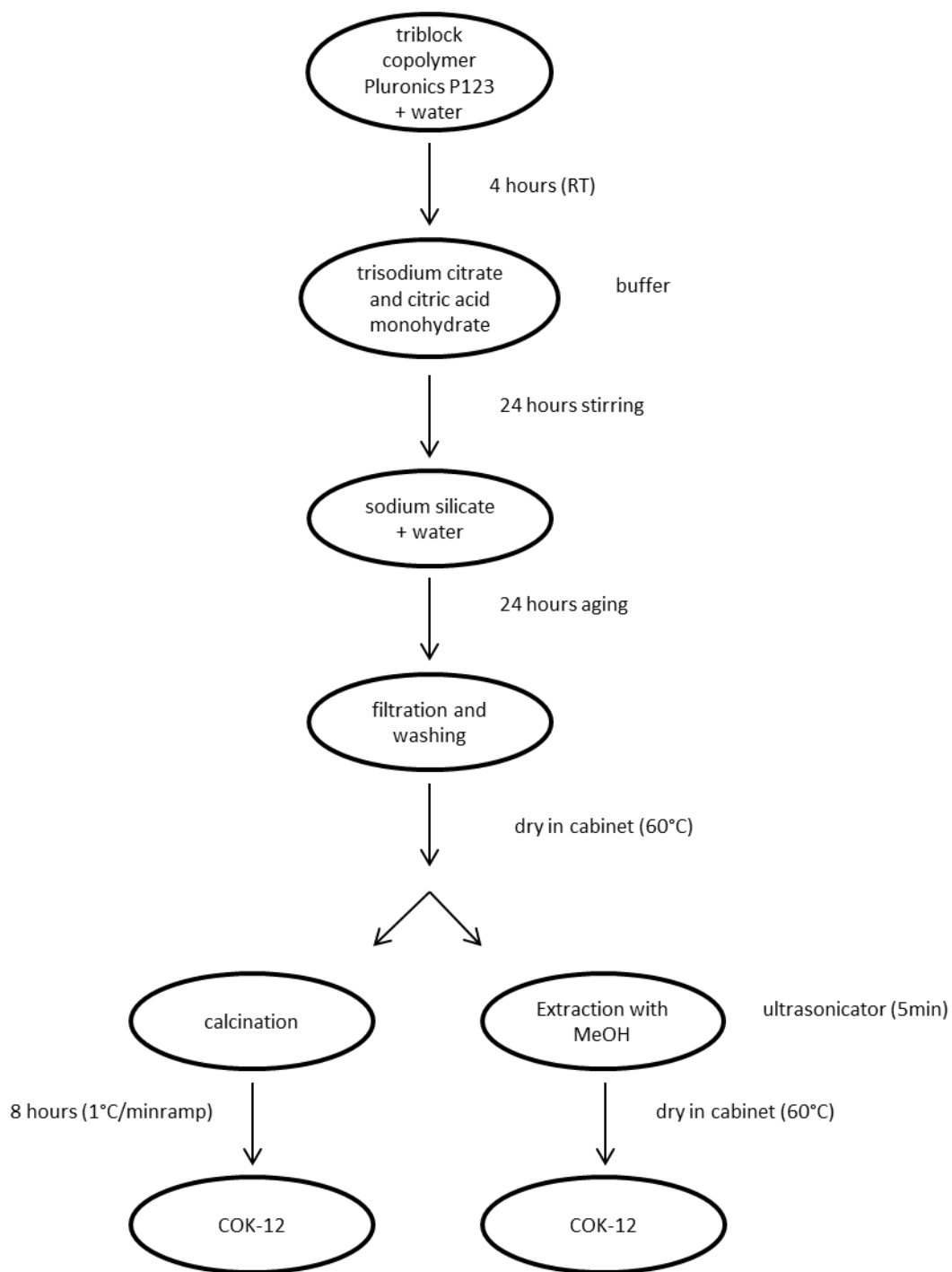


Figure 3.3 Schematic of COK-12 batch production with two different methods to remove the organic templating agent: calcination and extraction.

3.3 Spheres production

Spheres consisting of alginate or composites of alginate and COK-12 were produced by shaping and solidification in i) liquid nitrogen and ii) in a calcium chloride solution. The ratio of alginate to COK-12 was varied from 100% alginate to 70% COK-12. Sodium alginate (SIGMA-ALDRICH) was used, stirring with a magnetic stirrer to dissolve it in water. COK-12 calcined at 400°C was used and it was also dissolved in water using a magnetic stirrer and the ultrasonicator (5 min at room temperature).

For the spheres preparation a hose pump with speed of 35 rpm and a tube of a diameter of 3 mm was used to transport the solution.

In the first case, a small pan was filled with liquid nitrogen and the different solutions were dropped directly into the liquid nitrogen, so that the spheres were formed immediately. (Figure 3.4) The spheres were quickly stored in a freezer (-80°C) afterwards. After that they were put in a freeze dryer (Zirbus technologies, Sublimator VaCo 5) at 0.01 mbar and -80°C for 72 h. When this process was finished, the spheres were put in a 4% calcium chloride solution for 24h, so that the particles got crosslinked. Finally, they were washed with distilled water 5 or 6 times and put in the freeze dryer again for 72 h.

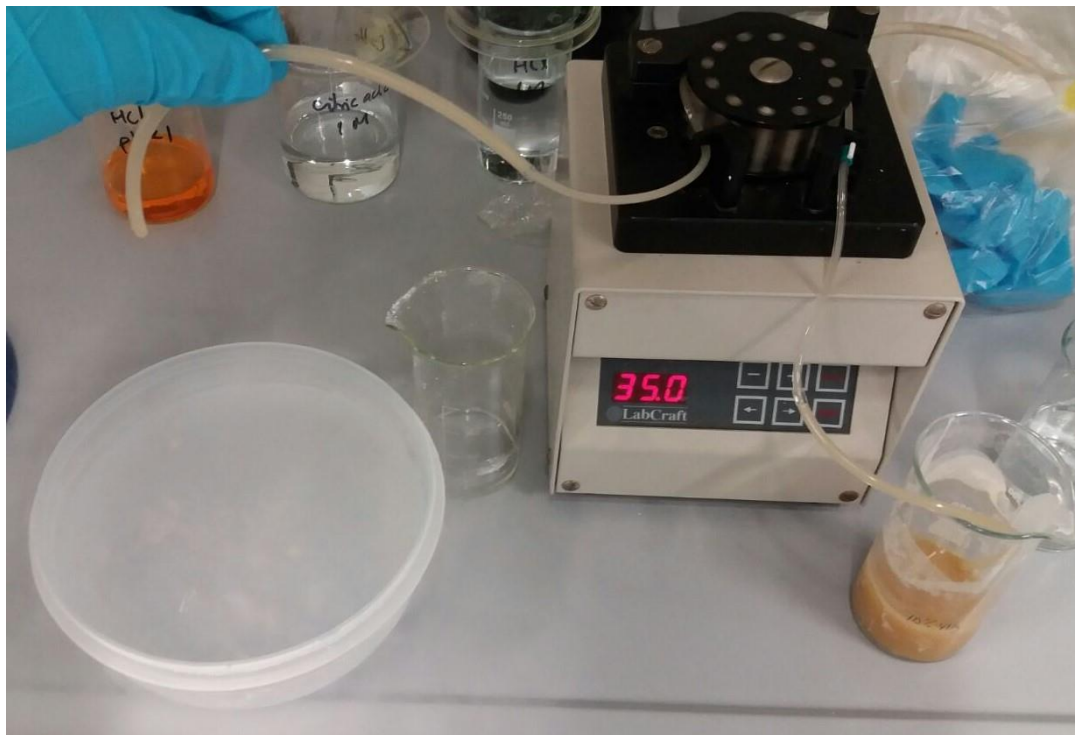


Figure 3.4 Spheres production with liquid nitrogen.

In the second case, the different solutions were dropped directly into a 4% calcium chloride solution and the spheres were formed immediately. (Figure 3.5) The solution with the spheres inside was aged for 24h and then washed with distilled water 5 or 6 times. Finally, they were out in the freeze dryer for 72 h.



Figure 3.5 Spheres production with calcium chloride.

Table 3.3 List of the different spheres produced with its compositions. Each type of spheres was done twice: one time only with calcium chloride (CaCl₂) and one time also with liquid nitrogen (N₂).

Spheres composition	Sample Code
Alginate [2%]	S_Alge_2%
Alginate [4%]	S_Alge_4%
Alginate [6%]	S_Alge_6%
Alginate [8%]	S_Alge_8%
(OMS (calcined at 400°C) (50%) + Alginate (50%)) [4%]	S_Alge_OMS(400)_4%
(OMS (calcined at 500°C) (50%) + Alginate (50%)) [4%]	S_Alge_OMS(500)_4%
(OMS (calcined at 400°C) (50%) + Alginate (50%)) [8%]	S_Alge_OMS(400)_8%
(OMS (calcined at 500°C) (50%) + Alginate (50%)) [8%]	S_Alge_OMS(500)_8%
(OMS (calcined at 400°C) (30%) + Alginate (70%)) [8%]	S_Alge70_OMS30(400)_8%
(OMS (calcined at 400°C) (40%) + Alginate (60%)) [8%]	S_Alge60_OMS40(400)_8%
(OMS (calcined at 400°C) (70%) + Alginate (30%)) [8%]	S_Alge30_OMS70(400)_8%

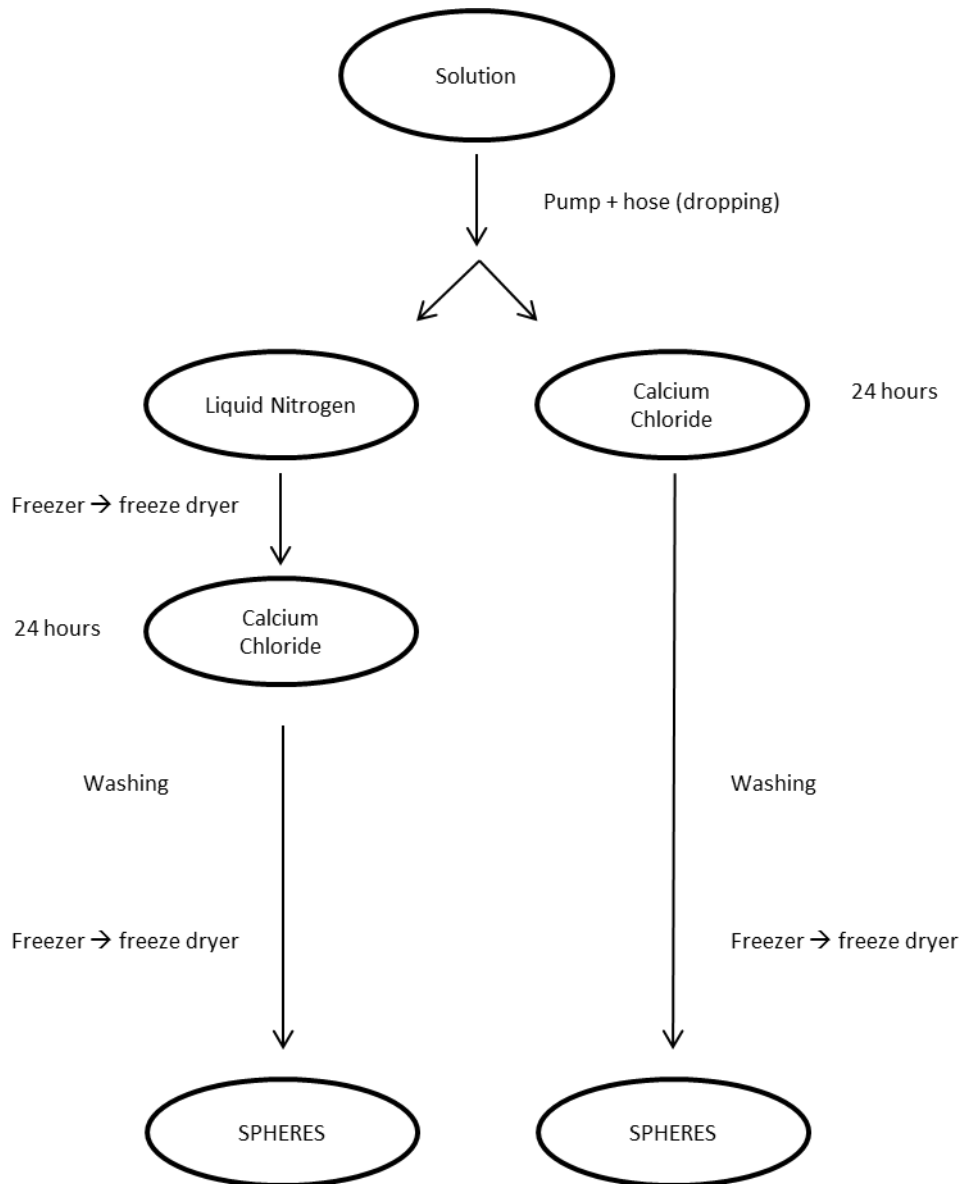


Figure 3.6 Schematic of spheres production with two different methods: with calcium chloride and with liquid nitrogen.

3.3.1 Solubility test

To check the stability of the spheres a solubility test was done. 50 ml of distilled water were put in a beaker with 0.15 g of S_AlgeOMS(500)_8%_N₂ and it was stirred with an agitation speed of 200 rpm, once for 48 h and once for 96 h. The same procedure was followed also with S_AlgeOMS(500)_8%_CaCl₂. For S_Alge_8%_CaCl₂ and S_Alge_8%_N₂, the same followed, but in this case only 10 ml water and 0.06 gr of the spheres were taken.

3.3.2 Water purification test

Nine solutions were prepared: three of methylene blue (MB), three of rhodamine 6G (RH) and three of congo red (CR). 20 ml of each solution were put in 9 glasses. Then the 3 different adsorbants: i) COK-12 calcined at 500 °C as powder, ii) spheres of 8% Alginate and COK-12 calcined at 500 °C produced with calcium chloride, and iii) spheres of 8% Alginate and COK-12 calcined at 500 °C produced with liquid nitrogen and calcium chloride were introduced. 100 mg of each adsorbant was introduced in one of each solution. The solutions were stirred for 2 h with an agitation speed of 400 rpm at room temperature (Figure 3.7). Then they were centrifuged at 5000 rpm for 5 min. The liquid part was separated from the solid part by decantation.



Figure 3.7 Solutions of methylene blue, rhodamine 6G and congo red stirred with different adsorbants: COK-12_500, S_Alg_OMS(500)_8%_N2, S_Alg_OMS(500)_8%_CaCl2.

The initial and final concentrations of MB, RH and CR were determined from their UV-vis absorbance using calibration curve method. UV/VIS/NIR spectrometer (Perkin Elmer Lambda 9) was used at $\lambda = 664, 526$ and $498 \mu\text{m}$ respectively.

The removal efficiency of each dye R_e (%) and the equilibrium adsorption capacity q_e (mg/g) where calculated as follows:

$$R_e = \frac{(C_i - C_e)}{C_i} * 100 \%$$

$$q_e = \frac{(C_i - C_e) * V}{m}$$

3.4 Tape production

To produce the films of the different compositions, a freezing process with liquid nitrogen was used. The set up shown in the picture consists in a metal box with a copper piece in the upper part, which had the form of the film. The metal box has a whole and trough this whole, the box was filled with liquid nitrogen with the help of a funnel. After 10 minutes a temperature of -28°C was reached. On the top of the copper piece, a metal sheet was placed and on top of it the solution was cast with the help of a small plastic dispenser with a small opening of 0.2mm, in order to obtain a very thin membrane. In around 1 minute, the film was completely frozen and placed in a freezer (-80°C) with the metal sheet. (Figure 3.6) Afterwards, it was put in the freeze dryer for 72 h. Finally, a very thin and flexible film was obtained.

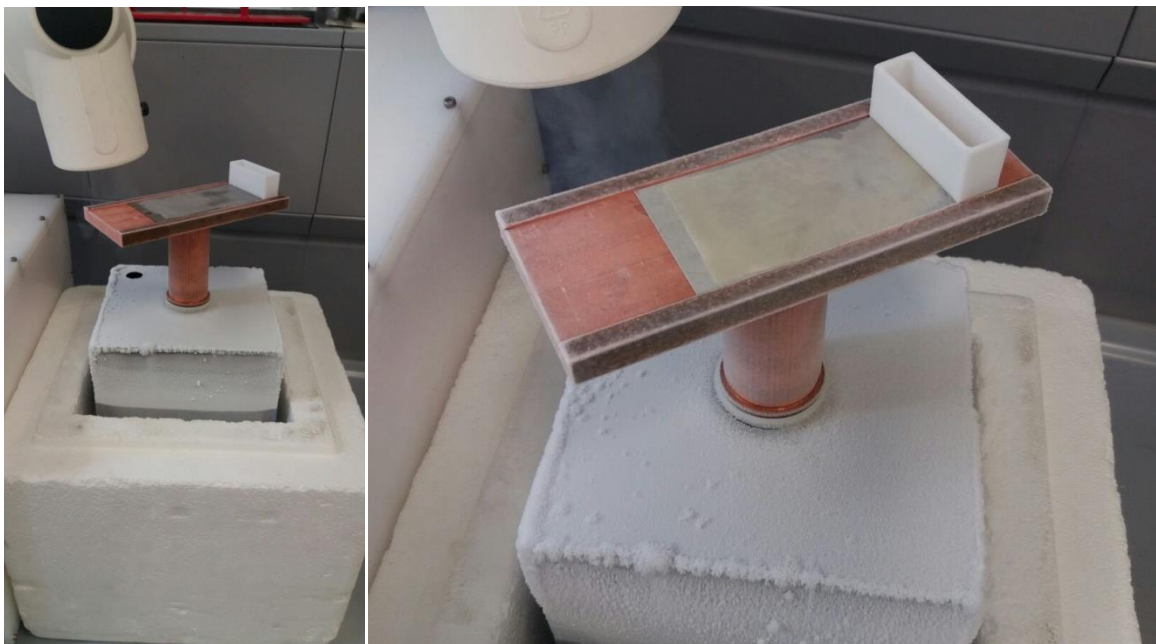


Figure 3.8 Films production with liquid nitrogen inside of the metal box.

Table 3.4 List of the different films produced with its compositions.

Films composition	Sample Codes
Alginate [4%]	T_Alq_4%
Alginate [8%]	T_Alq_8%
(OMS (calcined at 400°C) (50%) +Alginate (50%)) [8%]	T_Alq_OMS(400)_8%
(OMS (calcined at 400°C) (30%) +Alginate (70%)) [8%]	T_Alq70_OMS30(400)_8%
(OMS (calcined at 400°C) (40%) +Alginate (60%)) [8%]	T_Alq60_OMS40(400)_8%
(OMS (calcined at 400°C) (70%) +Alginate (30%)) [8%]	T_Alq30_OMS70(400)_8%
(OMS (calcined at 500°C) (10%) +Alginate (90%)) [8%]	T_Alq90_OMS10(400)_8%
(OMS (calcined at 500°C) (5%) +Alginate (95%)) [8%]	T_Alq95_OMS5(400)_8%

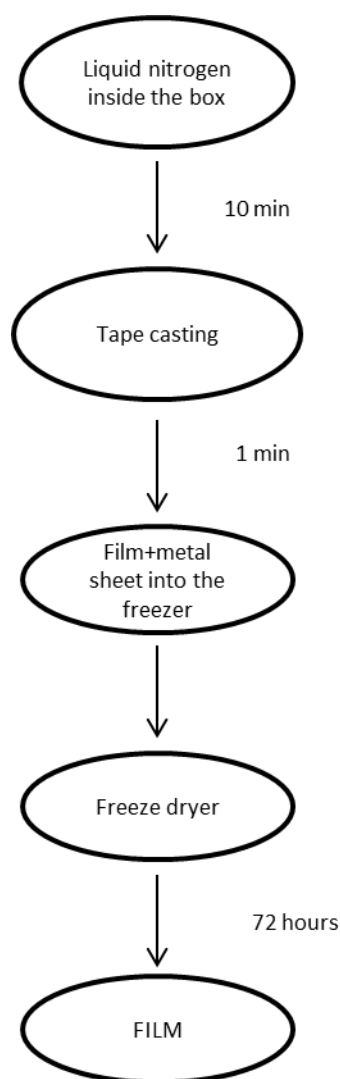


Figure 3.9 Schematic of films production.

4. Results and discussion

COK-12 was synthesized two times in batch (one of 25x the original and the other 10x the original) in order to guarantee the same properties of the material for all experiments. It was synthesized using two different methods of elimination of P123: i) calcination and ii) methanol extraction. To study the decomposition of the soft-template and the influence of synthesized COK-12, calcination was done at different temperatures, from 350°C up to 900°C. In addition, methanol extraction was investigated to try another method of soft-template removal that could be cheaper, faster, with less environmental impact and could have positive effect on surface characteristics. The results are compared to that obtained by calcination.

4.1 Influence of calcination temperature on pore morphology and surface characteristics

COK-12 was calcined at different calcination temperatures from 350°C up to 900°C. An optical image of the as-prepared powders is shown in Figure 4.1. All calcination temperatures lead to fine loosely agglomerated powders, while the color differs however. The COK-12 calcined at 350°C has a pale brown color. This color changes to white in the COK-12 calcined at higher temperatures.

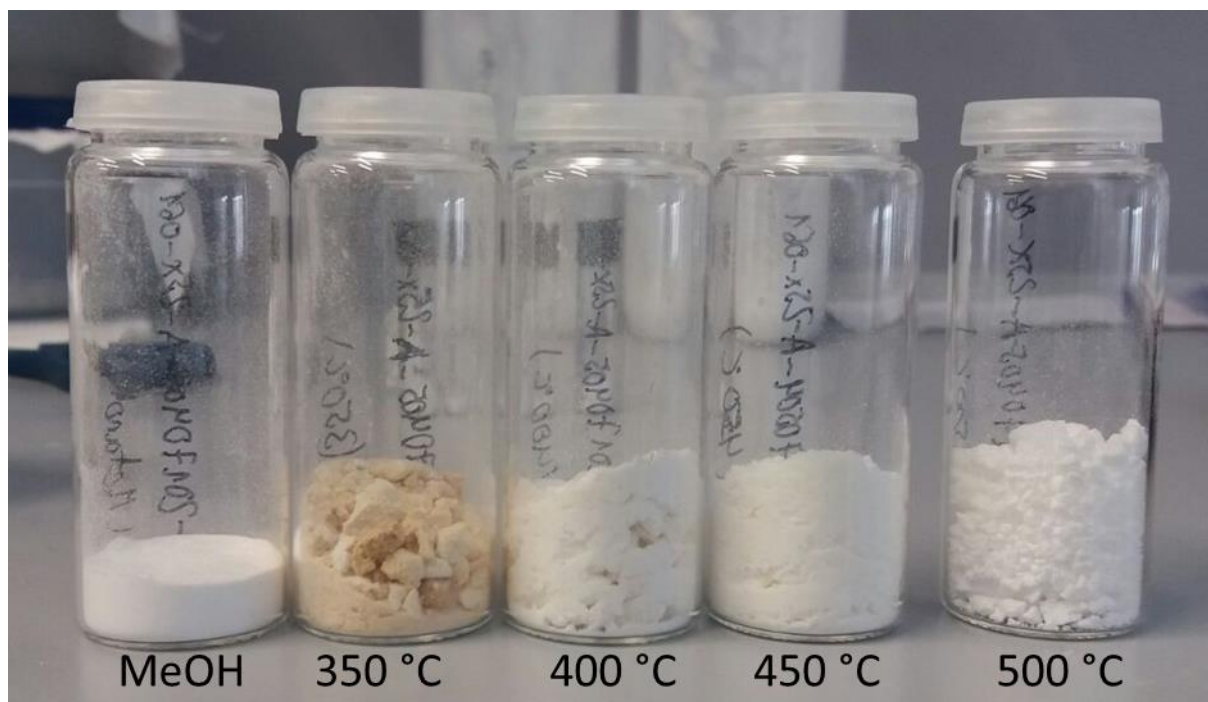


Figure 4.1 Comparison of COK-12 obtained with methanol extraction (left) and calcination at 350 °C, 400°C, 450 °C and 500 °C.

The main reason for the pale brown is the remaining semi-decomposed carbon content of the soft-template in the samples, which decreases with increasing calcination temperature from originally 29.8 wt% for the uncalcined sample to 1.9 wt% for a calcination temperature of 350°C to <0.1 wt% for 500 °C (Table 4.1). Thus, for calcination temperatures of >450 °C the soft-template can be fully removed. The hydrogen content was 1 wt% for a calcination temperature of 350 °C and it decreased a bit for higher calcination temperatures. The nitrogen and sulfur content was 0 wt% in all calcined samples. (Table 4.1)

Table 4.1 Nitrogen, carbon, hydrogen, sulfur, silicon and sodium content of COK-12 uncalcined, calcined at different temperatures from 350°C to 900°C and 2 extractions with methanol.

Substanz	% N ⁺	% C ⁺	% H ⁺	% S ⁺	% Na*	% Si*	%Na/(Na+Si)
uncalcined	0	29.86	5.65	0	-	-	-
350°C	0	1.92	1	0	0.14	35.70	0.0039
400°C	0	0.12	0.62	0	0.17	40.74	0.0042
450°C	0	0.15	0.57	0	0.27	40.71	0.0066
500°C	0	0.06	0.64	0	-	-	-
MeOH 10min	0	17.24	3.43	0	0.06	21.74	0.0028
MeOH 2x5min	0	21.69	4.04	0	0.06	29.03	0.0021

* content of Si and Na was measured with ICP-OES, ⁺ content of N, C, H and S was measured with elemental analysis

The influence of calcination temperature on the resulting pore structure within the COK-12 powders were analyzed by TEM, nitrogen sorption analysis and XRD at small angles.

TEM images of the COK-12 powders in dependence of the calcination temperature are shown in Figure 4.2, Figure 4.3, Figure 4.4 and Figure 4.5. These images show the periodicity and hexagonal ordering of the pores of COK-12. Uniform pore sizes can be observed.

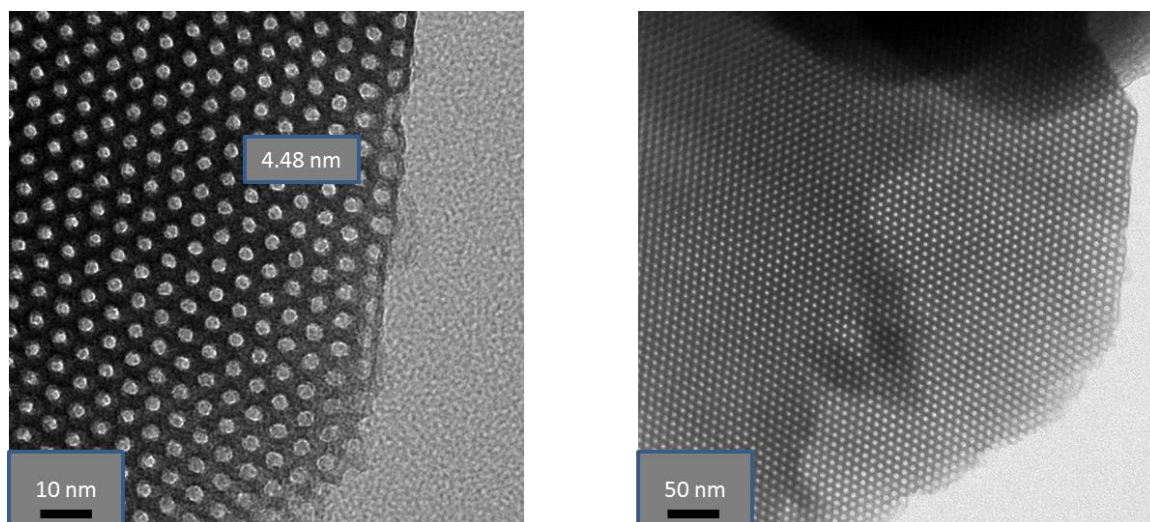


Figure 4.2 TEM micrographs of COK-12 calcined at 350°C.

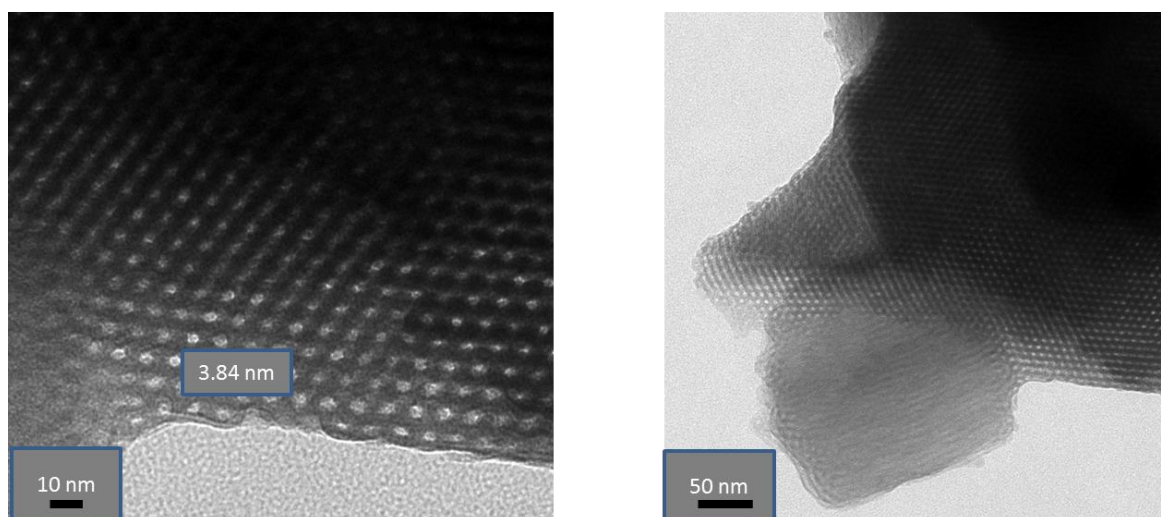


Figure 4.3 TEM micrographs of COK-12 calcined at 400°C.

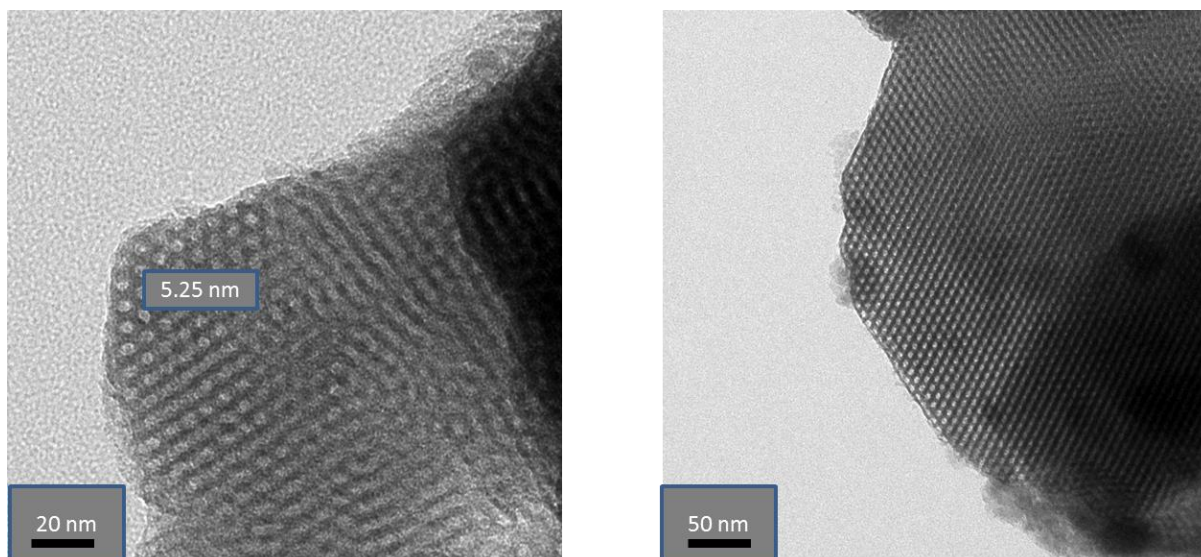


Figure 4.4 TEM micrographs of COK-12 calcined at 450°C.

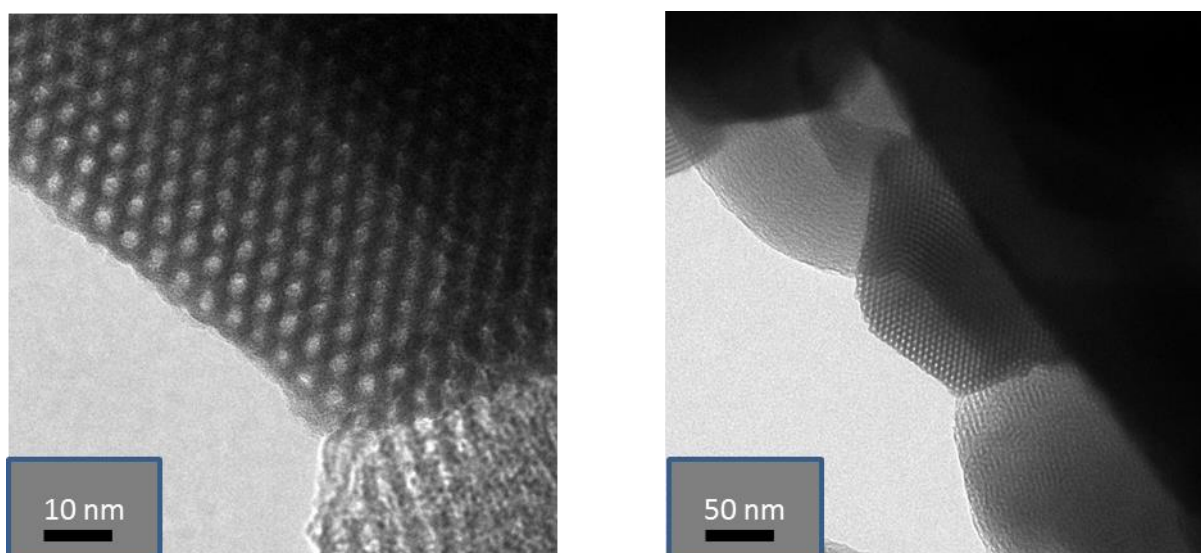


Figure 4.5 TEM micrographs of COK-12 calcined at 700°C.

Figure 4.6 shows the adsorption-desorption isotherms for the COK-12 powders calcined at temperatures from 350 °C up to 900 °C. The sample calcined at 700 °C should be repeated, because the adsorption-desorption isotherm seems to be wrong if it is compared to the other ones (Figure 4.6 f). For calcination temperatures up to 800 °C, type IV isotherm with a type H1 hysteresis are observed. This graphical overview reveals that the porous structure of COK-12 consists of an array of open cylindrical mesopores with a very narrow pore size distribution, confirmed by the steep adsorption branch of the hysteresis loop which indicates that capillary condensation occurs at a small relative pressure range.

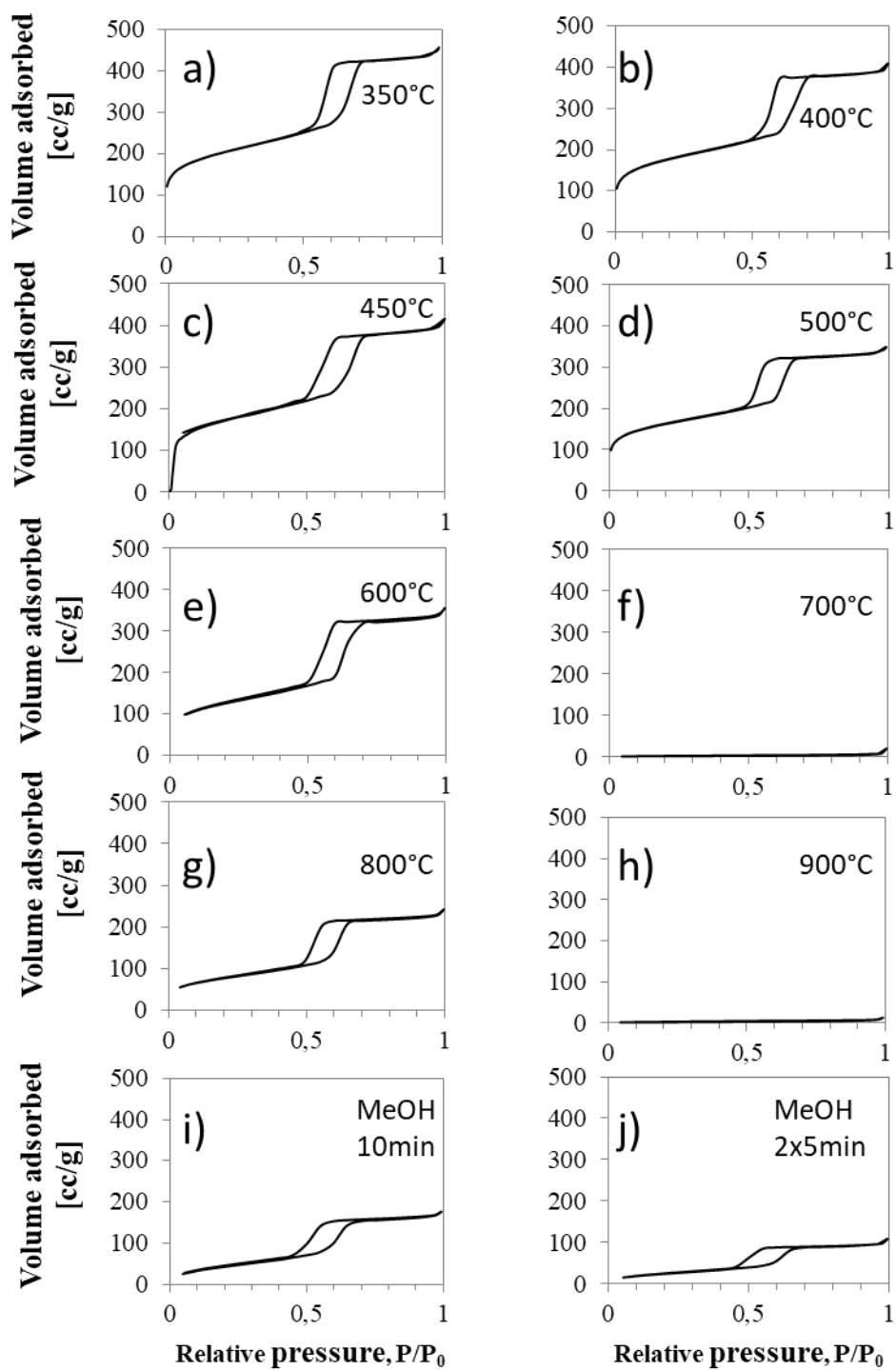


Figure 4.6 Nitrogen adsorption-desorption for COK-12 calcined at different temperatures from 350°C to 900°C and 2 extractions with methanol. The isotherms are all type IV with H1 hysteresis (apart from the higher temperatures, from 700°C up to 900°C), characteristic of mesoporous materials.

The pore size distributions, which were determined based on NLDFT calculations using the adsorption branch of the isotherms, are depicted in Figure 4.7. As already mentioned before, the sample calcined at 700 °C should be repeated, what can be also observed in the pore size distribution graph (Figure 4.7 f). With increasing the calcination temperature, the pore size decreases from 6.6 nm for 350 °C (Figure 4.7 a) to 6.1 nm for 800 °C (Figure 4.7 g). While the pore size distribution for 350°C shows a relatively sharp peak at 6.6 nm with a smaller shoulder around 6.1 nm, bimodal pore size distribution with peaks around 6.6 nm and 6.1 nm are observed for calcination temperatures of 400 and 450 °C (see Figure 4.7 b and c). For calcination temperatures same or greater than 500 °C only one single peak at 6.1 nm pore size is observed. These tendencies can be explained by the measurement of the carbon content. (Table 4.1) After calcination at 350 °C 1.9 wt% carbon from the soft-template (originally 29.9 wt%) are left in the sample, while the carbon content decreases with increasing calcination temperature to <0.1 wt% for 500 °C. According to Jammaer, et al.¹⁶ the pore size of OMS decreases by removing the soft-template due to a contraction of the pore. Thus, the two pore sizes of 6.6 and 6.1 nm stand for filled and unfilled pores respectively. If equal pore sizes are wanted, the calcination temperature must be 500 °C, because for calcination temperatures of 400 and 450 °C there is a bimodal pore size distribution.

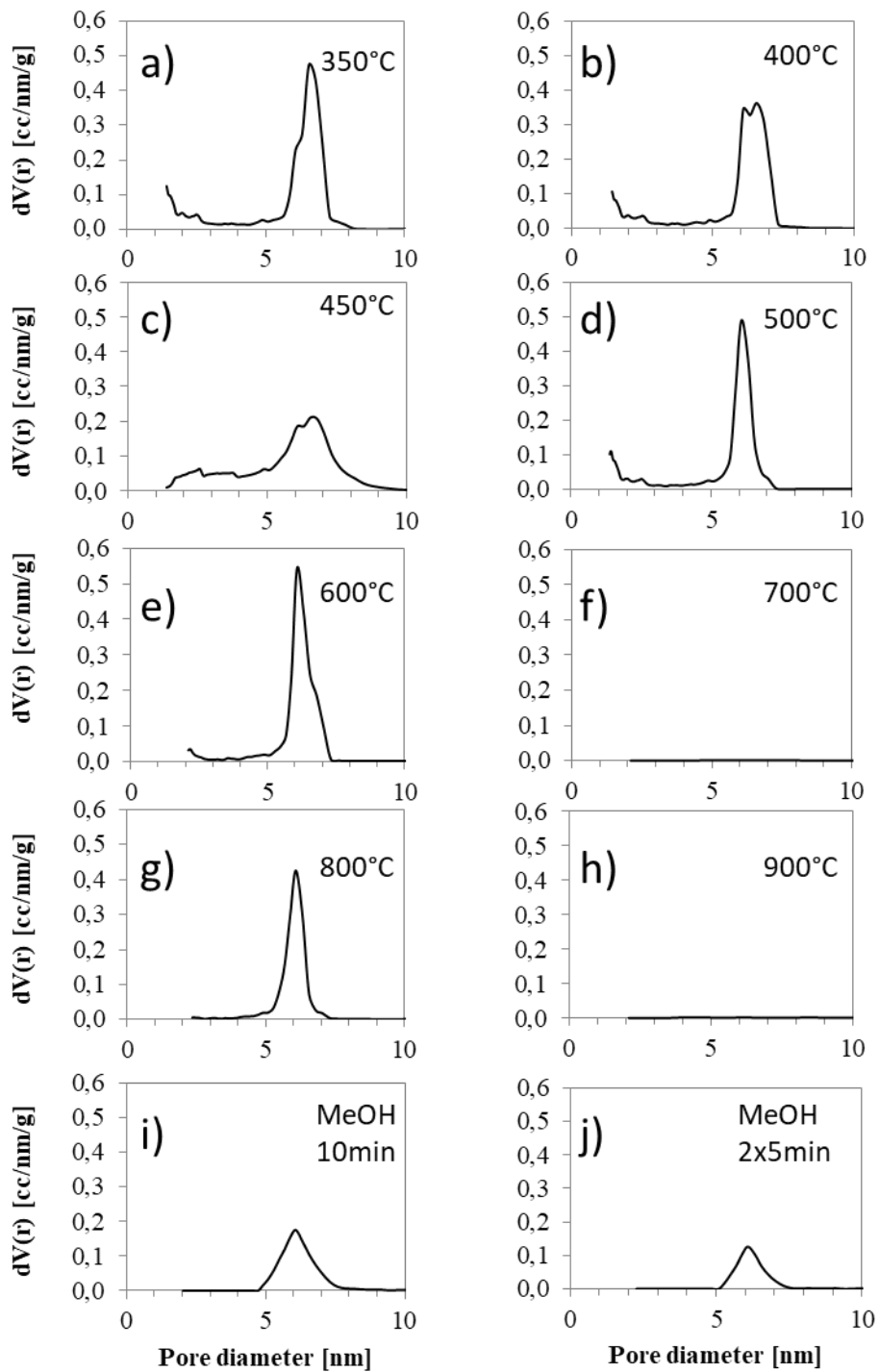


Figure 4.7 Pore size distribution of COK-12 calcined at different temperatures from 350°C to 900°C and 2 extractions with methanol as determined by the NLDFT method.

In accordance, the volume of nitrogen absorbed decreases with calcination temperature (Figure 4.6), which means that the pore volume decreases. This is caused by the decrease in size of the mesopores and a decrease in micro pore volume as summarized in Table 4.2.

Above a certain calcination temperature (around 650 °C) the pore volume decreases extremely, because of a collapse in mesoporosity. This is in agreement of the results of pore size distribution (Figure 4.7 f, g and h), where the peak of the pore size distribution in Figure 4.7, where the peak of the pore size distribution almost disappears for the higher calcination temperatures graphs.

Table 4.2 Surface area, pore width, pore volume and micropore volume of COK-12 calcined at different temperatures from 350°C to 900°C and 2 extractions with methanol.

Compound	d_{100}^a (nm)	Surface area ^b (m ² /g)	Pore width ^c (nm)	Pore volumen ^d (cc/g)	Microporevolume ^e (cc/g)
10min_Methanol	-	166.5	6.1	0.26	-
2*5min_Methanol	-	96.4	6.1	0.15	-
350°C	94.8	691.1	6.6	0.68	0.15
400°C	86.6	606.2	6.6	0.59	0.13
450°C	86.8	598.3	6.6	0.60	0.11
500°C	86.5	549.7	6.1	0.53	0.09
600°C	-	436.8	6.1	0.52	0.06
650°C	-	396.9	5.9	0.42	0.06
700°C	-	4.5	6.1	0.02	-
800°C	-	273.9	5.3	0.28	0.00
900°C	-	6.2	4.7	0.02	-

a Interplanar distance between (100) planes estimated by SAXRD

b Specific surface area estimated by BET

c Pore diameter estimated by NLDFT

d Pore volume estimated by NLDFT

e Micropore volume estimated by t-plot method

SAXRD experiments were done to study the pore ordering at the different calcination temperatures. In accordance to nitrogen sorption isotherms, from 350 °C until approximately 650°C, there is a first and high reflection at 2-Theta value of around 1° (Figure 4.8 a, b, c, d, e). This peak shows long-range hexagonally ordering and it is higher for lower calcination temperatures (Figure 4.8 a) than for the higher calcination temperatures (Figure 4.8 d). In addition, a second and even a third reflection can be observed at 2-Theta values of 1.7° and 2° respectively. The reflections follow the tendency $2\theta_1$; $2\theta_2 = \sqrt{3} * 2\theta_1$; $2\theta_3 = \sqrt{4} * 2\theta_1$, which satisfies the relation for p6m hexagonal symmetry. At calcination temperatures higher than 650°C, this peak disappears, because the pores are destroyed (Figure 4.8 f, g and h).

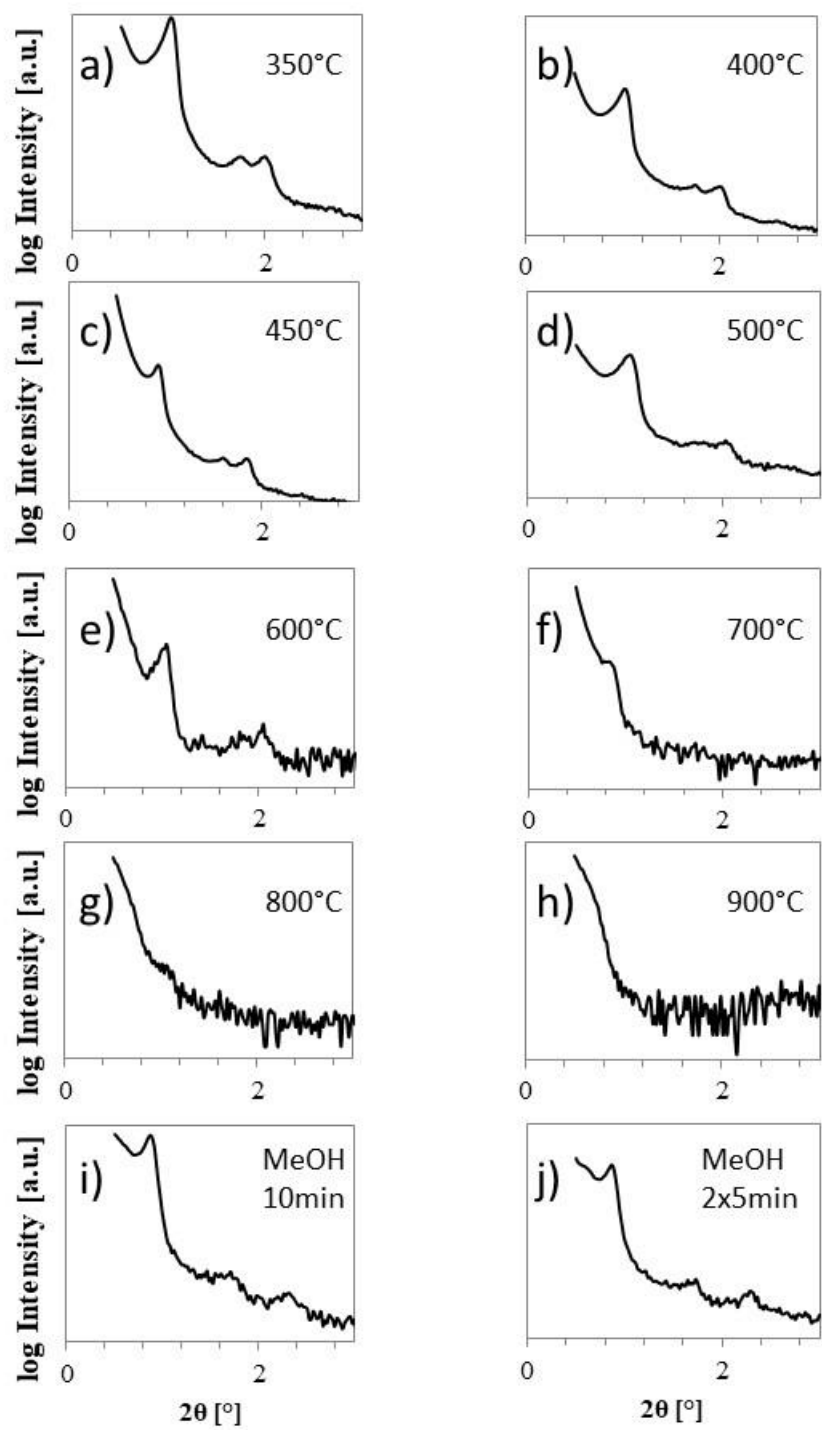


Figure 4.8 SAXRD patterns of COK-12 calcined at different temperatures from 350°C to 900°C and 2 extractions with methanol.

IR experiments were done to detect the chemical groups in dependence of the calcination temperature and methanol extraction method. The amount of Si-OH-groups decreases with the temperature as shown by a decrease in the detected vibrations band of $\nu_{\beta}\text{Si-Oat}$ 950 cm^{-1} (Figure 4.8). Elemental analysis supports the IR experiments. The measured hydrogen content decreases from 1 wt% for $350\text{ }^{\circ}\text{C}$ to 0.6 wt% for 500°C with increasing calcination temperature (see Table 4.1).

Remaining carbon and SiOH-groups are a very important aspect for further surface functionalization of COK-12, because there is a need of Si-OH-groups for further surface functionalization with functional organic groups, which could be relevant e.g. for medical applications, sorption, drug delivery or for the use as catalyst support. Therefore, the use of COK-12 calcined at lower temperatures is preferred for the further production of spheres and membranes, in order to preserve the Si-OH-groups.

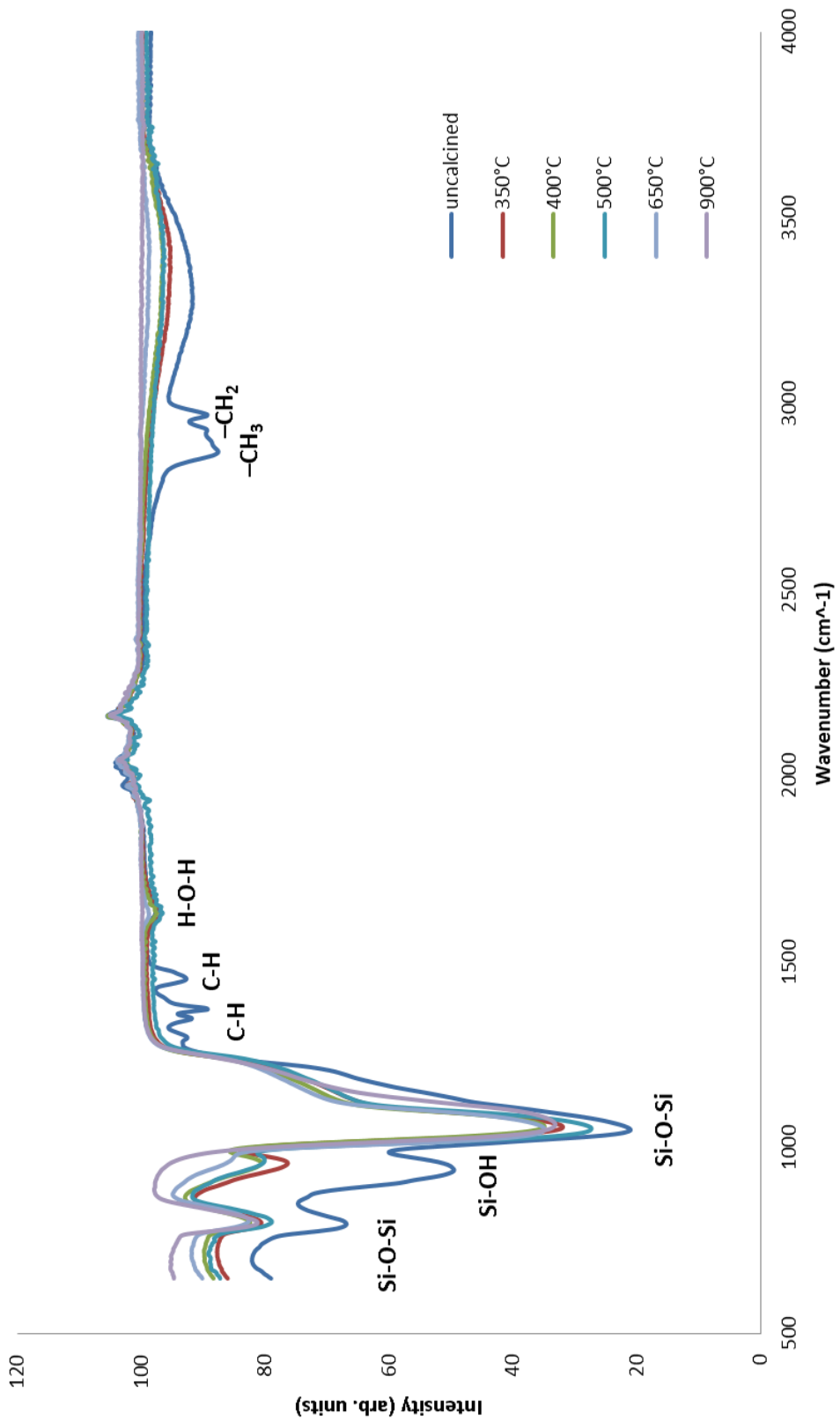


Figure 4.9 ATR-IR graph for COK-12 uncalcined and calcined at 350 °C, 400 °C, 500°C, 650°C and 900 °C.

4.2 Influence of extraction on pore morphology and surface characteristics

As mentioned above methanol extraction was investigated to try another method of soft-template removal that could be cheaper, faster, with less environmental impact and could have positive effect on surface characteristics. The results are compared to that obtained by calcination.

COK-12 synthesized with methanol extraction shows a very fine powder without large agglomerates as observed for the calcined samples (Figure 4.1).

Although the COK-12 synthesized with methanol extraction has a white color (Figure 4.1), the carbon content (17.24 wt%; 21.69 wt%) is much higher than in the COK-12 calcined at 350°C (1.92 wt%). The white color is due to the fact that the carbon only gets the brown color if it's burned and in the methanol extraction there is no heat contribution. The hydrogen content is also higher in the COK-12 synthesized with methanol extraction (3.43 wt%; 4.04 wt%) than in the calcined COK-12 (≤ 1 wt%). The nitrogen and sulfur content was also 0 wt% in the methanol extracted samples, which is in agreement to the calcined samples. (Table 4.1)

In accordance with calcination temperature investigations, nitrogen sorption measurements were done for COK-12 prepared by methanol extraction method as shown in Figure 4.6 i, j. For both extractions, type IV isotherm with a type H1 hysteresis are observed. Their shapes are not that sharp as after calcination. However, by increasing the extraction time to 10 min the shapes get more faceted. In total the hysteresis loops are shifted to lower adsorbed gas values in comparison to the calcined ones. This is in accordance to an increase pore volume from 0.15 to 0.26 cm³/g for 2x5 min and 10 min respectively. In comparison to calcined COK-12 (e.g. 0.60 cm³/g for calcination temperature of 450 °C) the value is still very low. (Table 4.2)

The pore size distributions, which were determined based on NLDFT calculations using the adsorption branch of the isotherms, are depicted in Figure 4.7. The maximum pore size is around 6.1 nm. The peaks are lower and broader in comparison to the graphs obtained of the calcined samples, which indicates a broader pore size distribution with pore sizes from 5 nm to 6 nm. This is in agreement with their low pore volumes, caused by the incompletely removed soft-template, which was proven by elemental analysis.

XRD at small angle diffractograms are shown in Figure 4.8i, j. The first reflection at 0.8 ° is smaller at 2 theta values than in the graphs of low calcination temperatures (Figure 4.8 a, b), which shows smaller pore sizes. There is also noise in both methanol extraction graphs and the second and third peak are not clearly recognizable (Figure 4.8i, j). This means that the pore ordering is less in COK-12 produced with methanol extraction than in COK-12 produced with low temperature calcination.

IR measurements were used to study the chemical composition. Antisymmetric stretching vibration, which correspond to Si-O-Si groups, can be observed in the uncalcined, calcined and extracted COK-12. Also in-plane stretching vibration corresponding to Si-OH groups. Different carbohydrate groups are present, in the uncalcined COK-12. The peaks of those carbohydrates are lower for the extractions (lower for the extraction of 10 min than 2x5 min) and in the calcined COK-12 at 500 °C those peaks disappear. The carbohydrate groups are $-CH_2$ (symmetric stretching vibration) and $-CH_3$ (antisymmetric stretching vibration).

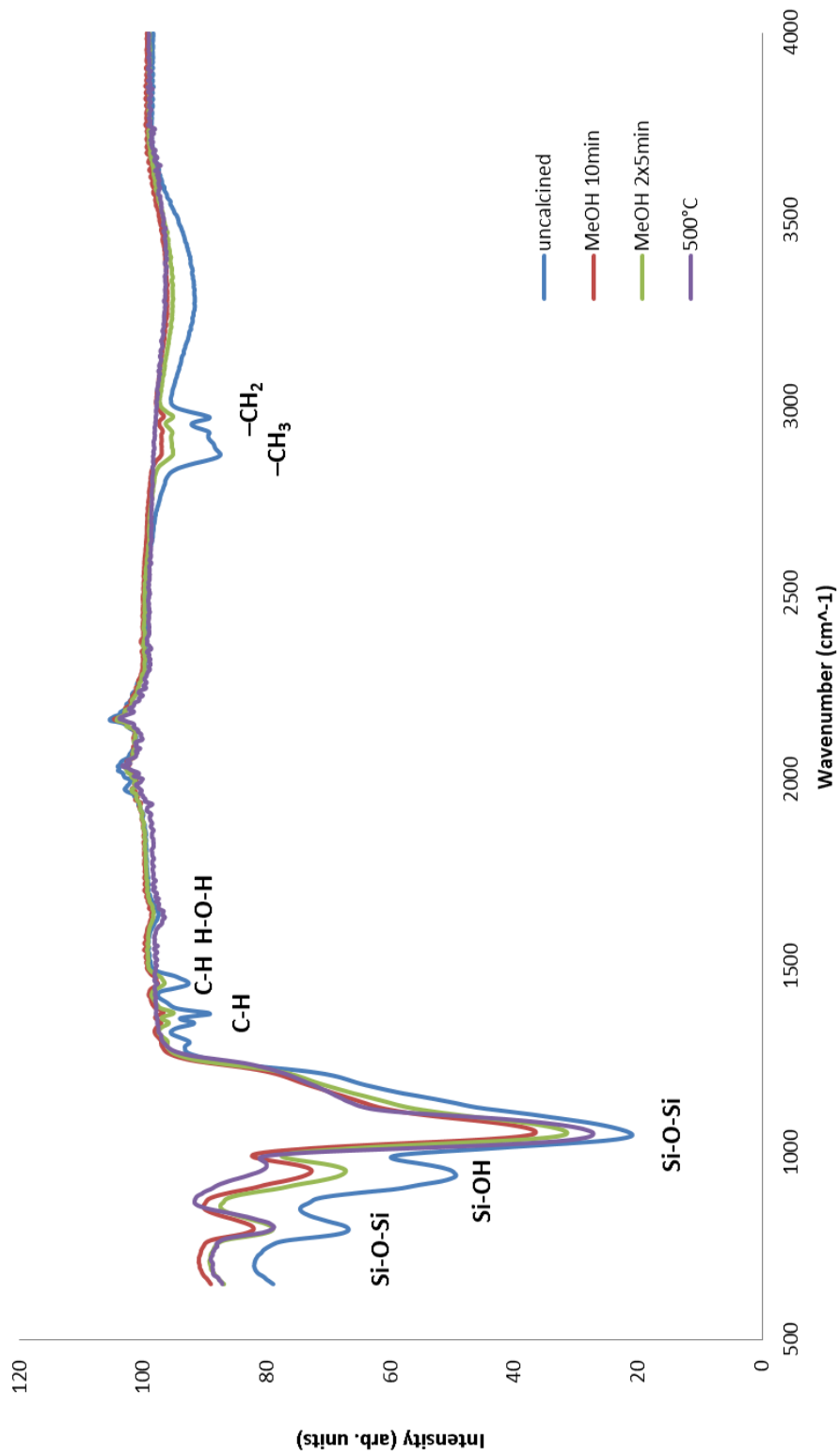


Figure 4.10 ATR-IR graph for COK-12 uncalcined, calcined at 500 °C and COK-12 produced with 10 min and 2x5 min methanol extraction.

4.3 Spheres

Spheres consisting of alginate or composites of alginate and COK-12 were produced by shaping and solidification in i) liquid nitrogen and ii) in a calcium chloride solution. The ratio of alginate to COK-12 was varied from 100% alginate to 70% COK-12.

4.3.1 Spheres analysis

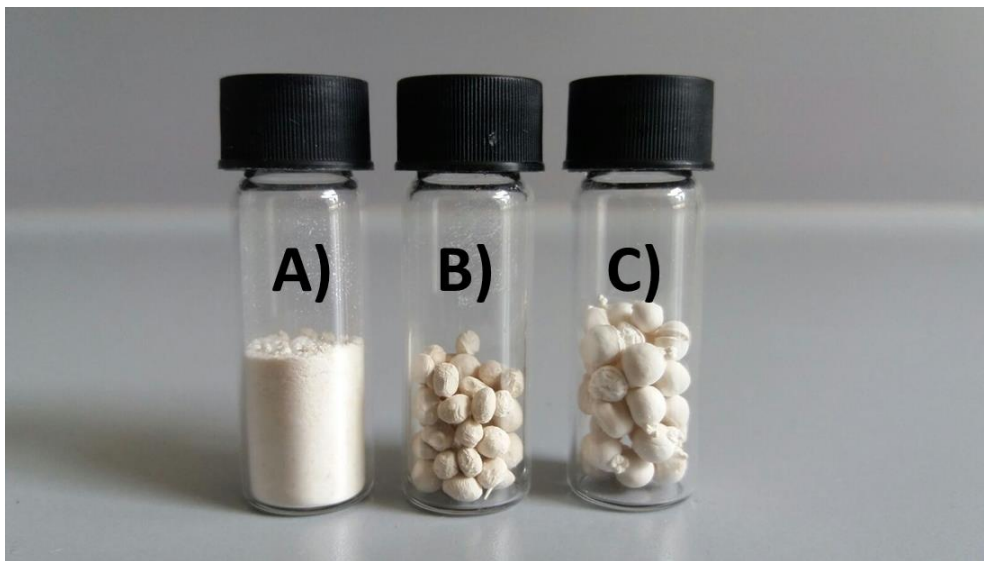


Figure 4.11 Comparison of COK-12 calcined at 400 °C (A), S_Al70_OMS30(400)_8%_CaCl2 and S_Al70_OMS30(400)_8%_N2.

Spheres produced only with calcium chloride have a diameter which vary from 2 to 4 mm and the ones produced also with liquid nitrogen have a diameter which vary from 3 to 5 mm. This variation depends on the different compositions of the spheres. With a higher percentage of alginate the spheres are bigger, which is due to the density of the solution: at higher density the drops coming out of the hose are bigger. It can be observed in Figure 4.12 and the composition of each of those spheres are compiled in Table 4.3.

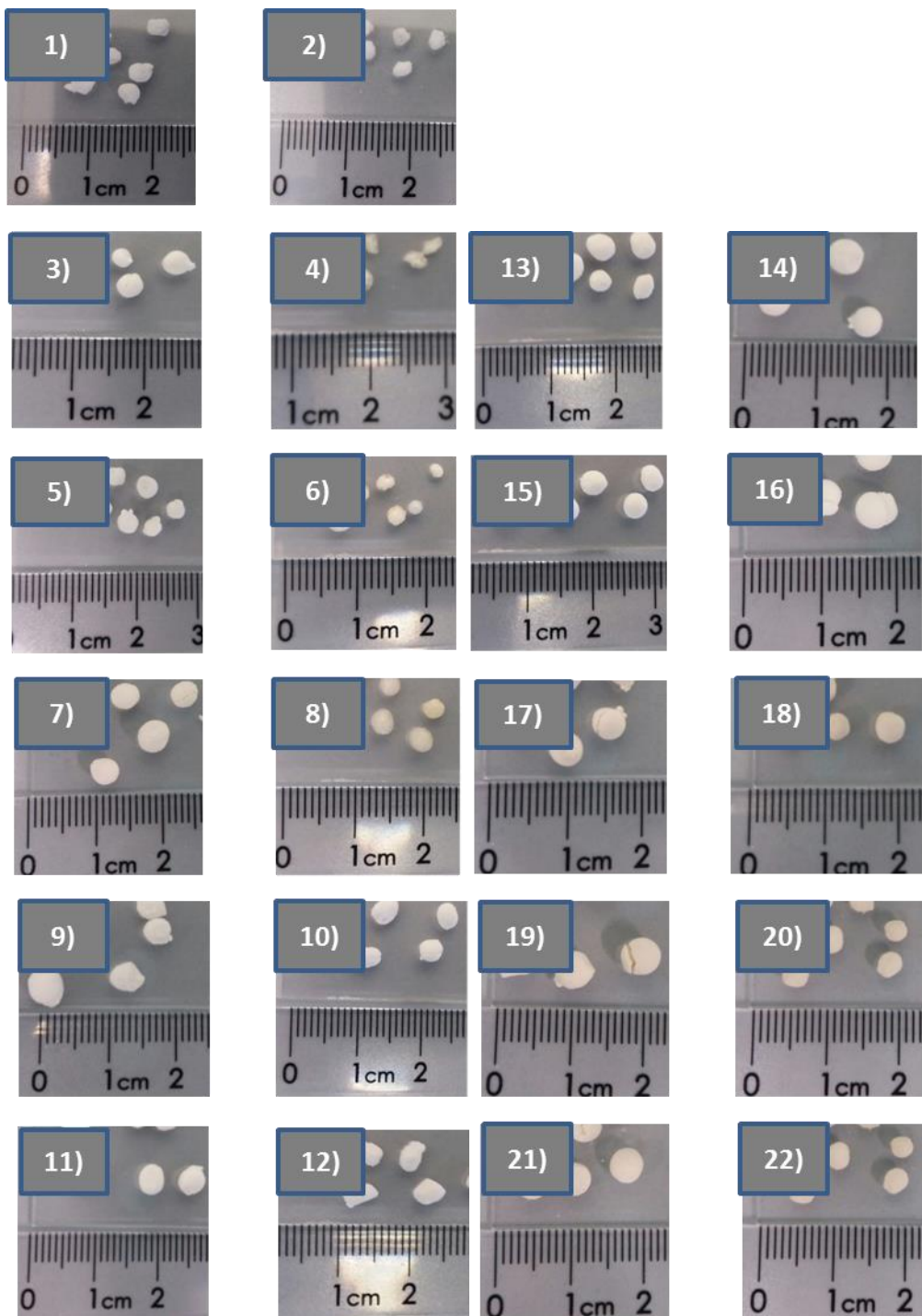


Figure 4.12 Pictures of all spheres done for this thesis. The sample codes can be read on Table 4.3.

Table 4.3 Sample codes according to the number of the spheres shown in Figure 4.12.

Number	Sample Code
1	S_Alg_2%_N ₂
2	S_Alg_2%_CaCl ₂
3	S_Alg_4%_N ₂
4	S_Alg_4%_CaCl ₂
5	S_Alg_6%_N ₂
6	S_Alg_6%_CaCl ₂
7	S_Alg_8%_N ₂
8	S_Alg_8%_CaCl ₂
9	S_Alg_OMS(400)_4%_N ₂
10	S_Alg_OMS(400)_4%_CaCl ₂
11	S_Alg_OMS(500)_4%_N ₂
12	S_Alg_OMS(500)_4%_CaCl ₂
13	S_Alg_OMS(400)_8%_N ₂
14	S_Alg_OMS(400)_8%_CaCl ₂
15	S_Alg_OMS(500)_8%_N ₂
16	S_Alg_OMS(500)_8%_CaCl ₂
17	S_Alg70_OMS30(400)_8%_N ₂
18	S_Alg70_OMS30(400)_8%_CaCl ₂
19	S_Alg60_OMS40(400)_8%_N ₂
20	S_Alg60_OMS40(400)_8%_CaCl ₂
21	S_Alg30_OMS70(400)_8%_N ₂
22	S_Alg30_OMS70(400)_8%_CaCl ₂

The spheres S_Al_g_4%_N₂ (Figure 4.13) and S_Al_g_8%_N₂ (Figure 4.14) show an open porosity, but the difference is that the spheres with 8 wt% alginate have a bigger porosity inside compared to the spheres with 4 wt% alginate.

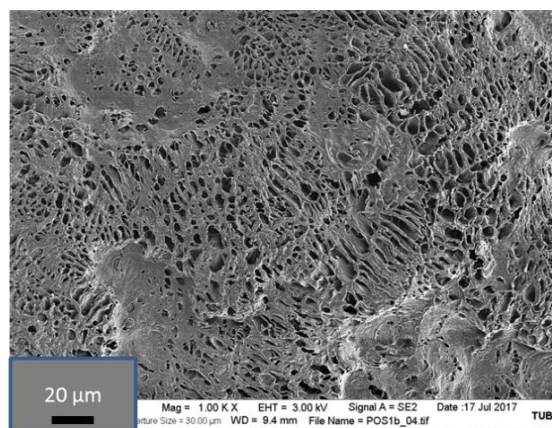
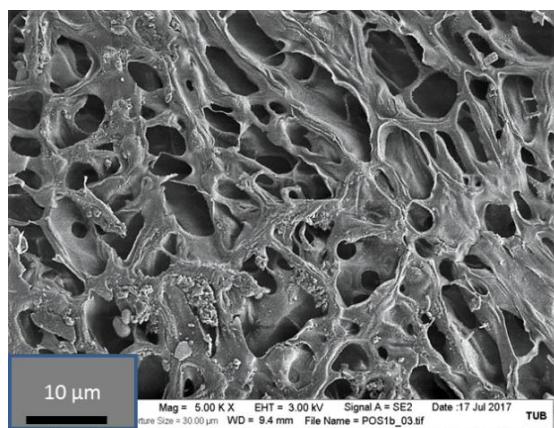


Figure 4.13 REM S_Al_g_4%_N₂.

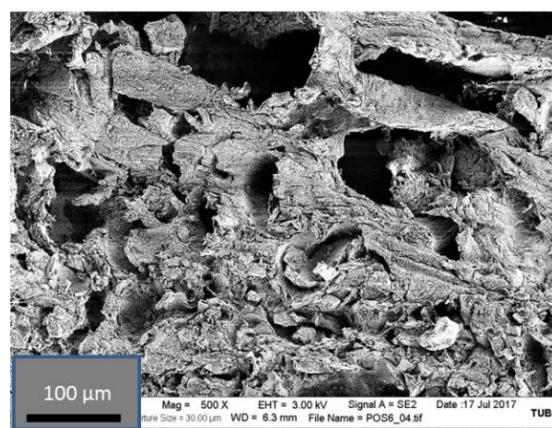
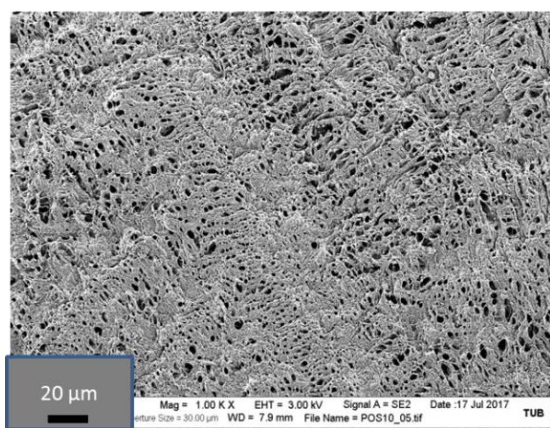
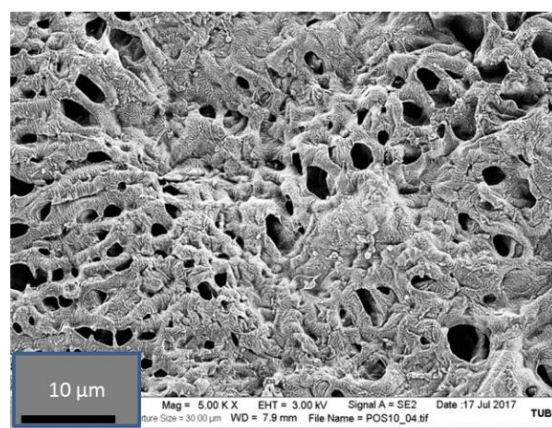
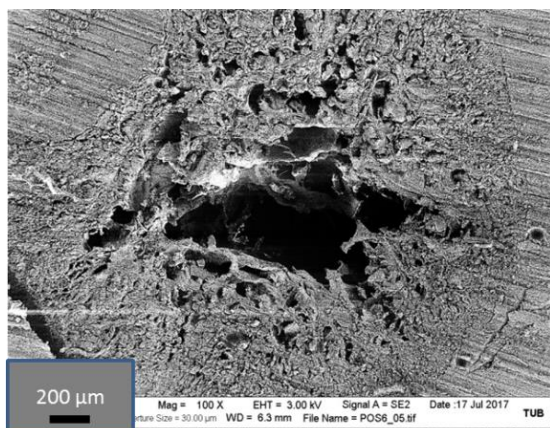


Figure 4.14 REM S_Al_g_8%_N₂.

The spheres S_Al_g_4%_CaCl₂ (Figure 4.15) and S_Al_g_8%_CaCl₂ (Figure 4.16) have a closed surface and there are less pores inside compared to the spheres produced with liquid nitrogen commented above.

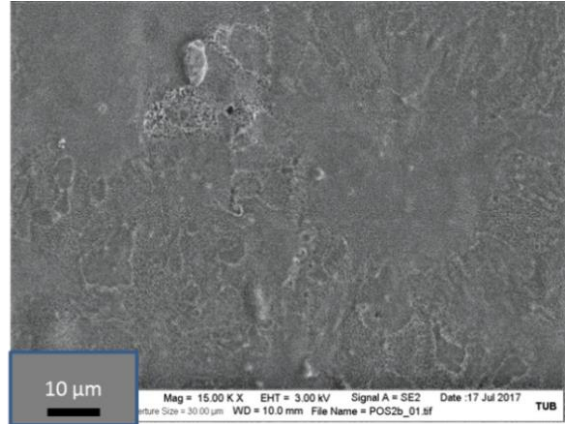
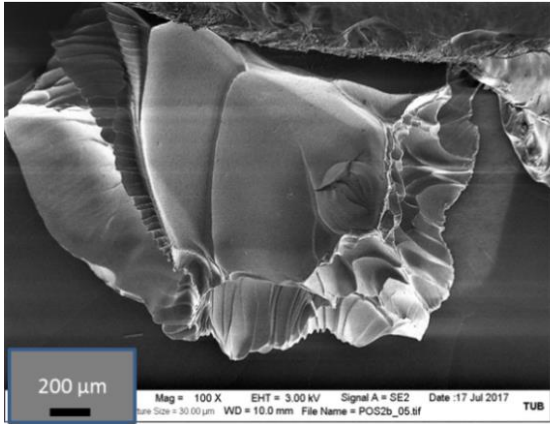


Figure 4.15 REM S_Al_g_4%_CaCl₂.

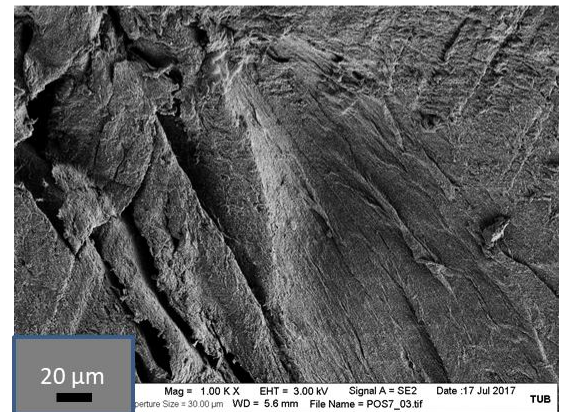
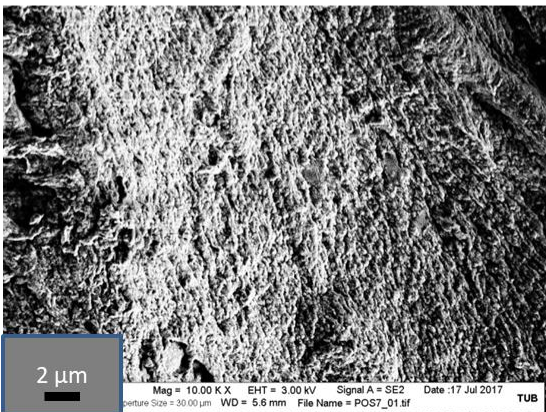
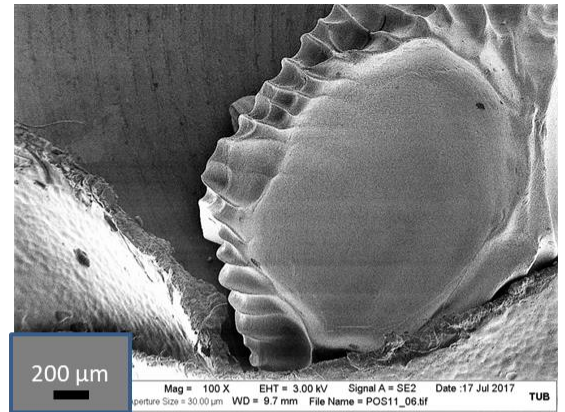
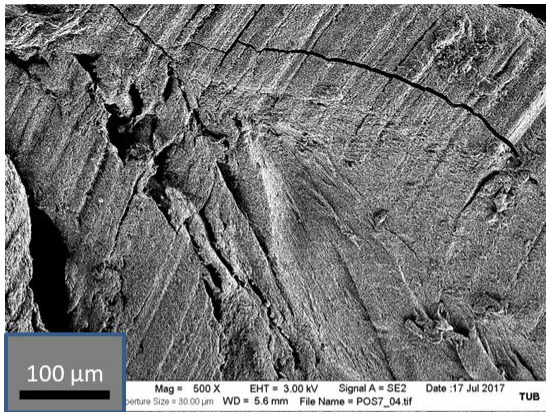


Figure 4.16 REM S_Al_g_8%_CaCl₂.

The spheres S_Al_g_OMS(500)_8%_CaCl₂ (Figure 4.17) have much less pores than the same type of spheres produced with liquid nitrogen (Figure 4.18). The pores are bigger in the spheres produced with liquid nitrogen and the reason could be that the alginate does not make so many lamellae, because it is covering the OMS. Bigger pores could be a positive aspect for some applications. It can also be observed that the roughness is increased after adding the OMS. The OMS is apparently divided up equally all over the sphere, but in the spheres produced with liquid nitrogen there are some places where there is more OMS in the close area.

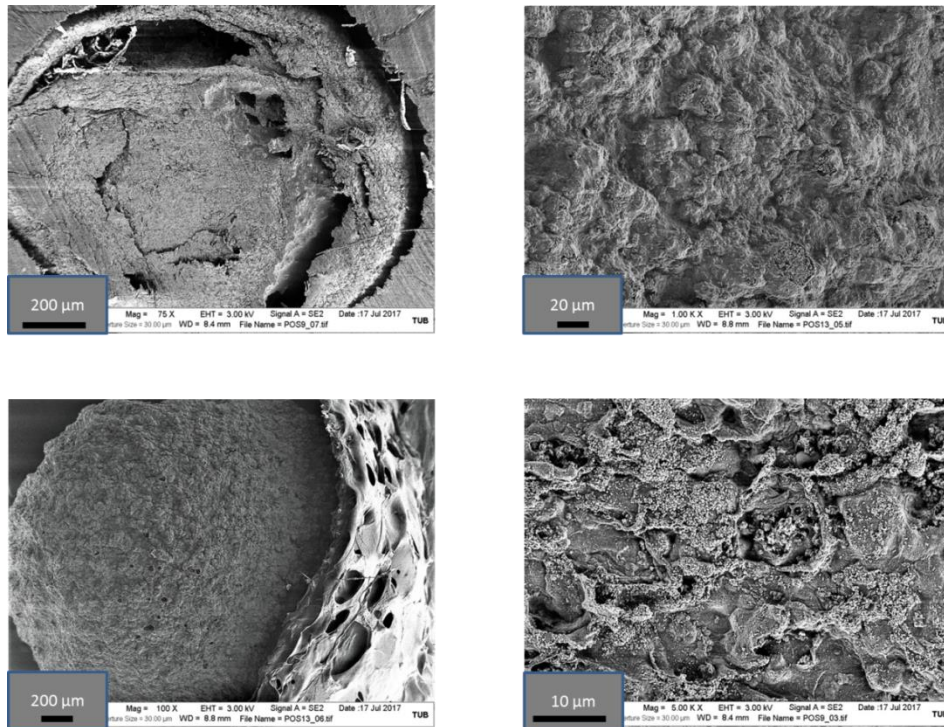


Figure 4.17 REM S_Al_g_OMS(500)_8%_CaCl₂.

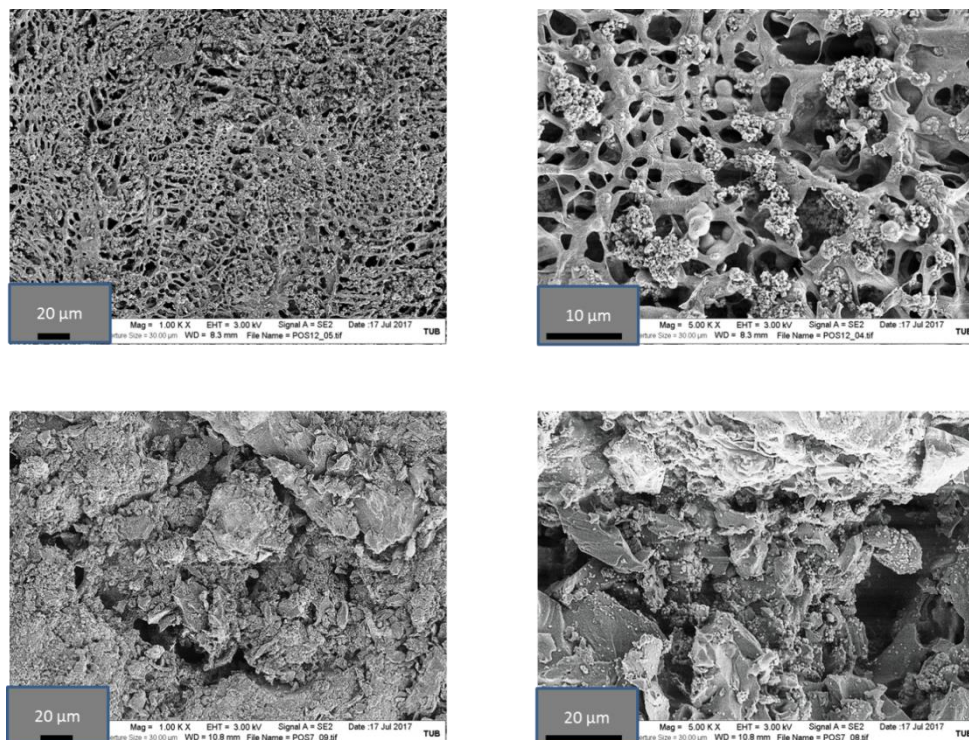


Figure 4.18 REM S_Al_g_OMS(500)_8%_N₂.

In Tables 4.4 and 4.5 there can be found some information about the specific surface area, pore diameter and pore volume. These measurements should have been done for every type of spheres produced for this thesis, but some of them are missing due to a reason of time. Nevertheless, some conclusions can be taken from the information shown on both tables.

The surface area of the spheres is considerably bigger in the spheres produced with liquid nitrogen, compared to the spheres produced without liquid nitrogen. The spheres containing COK-12 calcined at 500 °C have a bigger surface area compared to the spheres containing COK-12 calcined at 400 °C, but the difference is not as big as the one just commented. Another aspect which can be observed is that the spheres containing a bigger percentage of OMS have a bigger surface area compared to the spheres with a lower OMS percentage.

The pore diameters range from 6.1 to 6.6 nm, but a clear tendency influenced by the parameters changed in each type of spheres can not be observed.

The pore volume of the spheres produced with liquid nitrogen and calcium chloride is bigger than the volume of the spheres produced only with calcium chloride.

Table 4.4 Surface area, pore width, pore volume and micropore volume of spheres with COK-12 calcined at 400 °C.

Compound (400 °C)	d_{100}^a (nm)	Surface area ^b (m ² /g)	Pore width ^c (nm)	Pore volumen ^d (cc/g)
S_Al _g _OMS(400)_4% (N)	86.6	-	6.6	0.59
S_Al _g _OMS(400)_4% (CaCl ₂)	-	56.10	6.6	0.10
S_Al _g _OMS(400)_8% (N)	-	161.03	6.1	0.23
S_Al _g 30_OMS70(400)_8% (CaCl ₂)	-	216.26	65.6	0.34

a Interplanar distance between (100) planes estimated by SAXRD

b Specific surface area estimated by BET

c Pore diameter estimated by NLDFT

d Pore volume estimated by NLDFT

Table 4.5 Surface area, pore width, pore volume and micropore volume of spheres with COK-12 calcined at 500 °C.

Compound (500 °C)	d ₁₀₀ ^a (nm)	Surface area ^b (m ² /g)	Pore width ^c (nm)	Pore volumen ^d (cc/g)
S_Alg_OMS(500)_4% (N)	-	187.89	60.8	0.25
S_Alg_OMS(500)_4% (CaCl ₂)	-	61.32	65.6	0.103
S_Alg_OMS(500)_8% (N)	-	169.18	6.1	0.212

a Interplanar distance between (100) planes estimated by SAXRD

b Specific surface area estimated by BET

c Pore diameter estimated by NLDFT

d Pore volume estimated by NLDFT

In Figures 4.19 and 4.20 four adsorption-desorption isotherms can be observed: one of the COK-12 powder (a), one of the spheres produced with liquid nitrogen and calcium chloride containing the same COK-12 powder (b), the same spheres but produced without liquid nitrogen (c) and other spheres with a higher COK-12 composition (d).

The COK-12 powder show the biggest volume of nitrogen adsorbed. In Figure 4.20 the isotherm of the spheres produced with liquid nitrogen (b) show a bigger volume adsorbed, compared to the spheres produced without liquid nitrogen (c), which supports the results of Tables 4.4 and 4.5 commented above. In Figure 4.19 the opposite can be observed, the volume adsorbed is bigger in the spheres produced without liquid nitrogen, but this could be due to a measurement or label error. The spheres with a higher COK-12 composition show a bigger volume of nitrogen adsorbed, which makes sense, because there are more pores.

The pore size distributions corresponding to the four samples commented above, which were determined based on NLDFT calculations using the adsorption branch of the isotherms, are depicted in Figures 4.21 and 4.22.

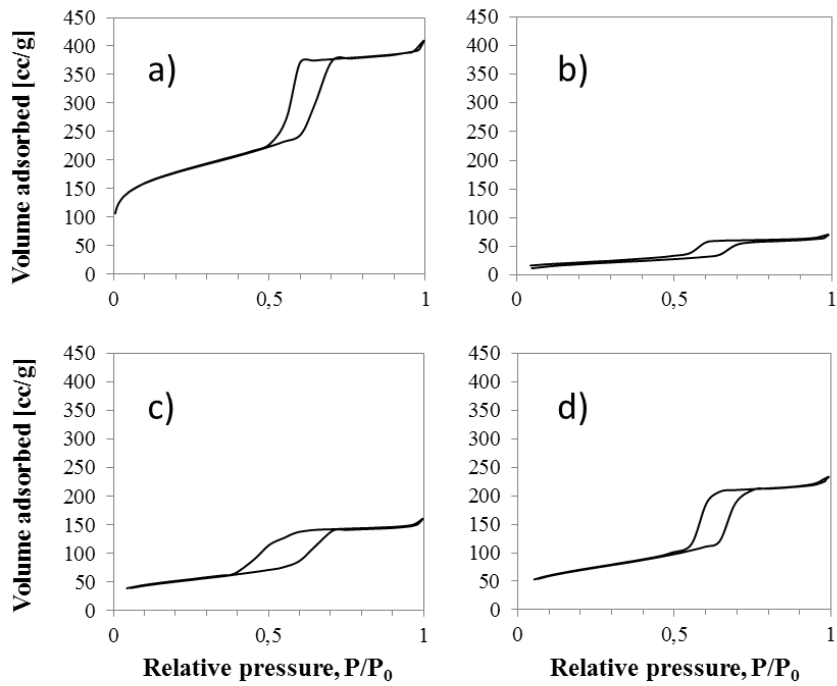


Figure 4.19 Nitrogen adsorption-desorption for a)COK-12_400, b)S_Alq_OMS(400)_4%_CaCl2, c)S_Alq_OMS(400)_8%_N2, d)S_Alq30_OMS70(400)_8%_CaCl2.

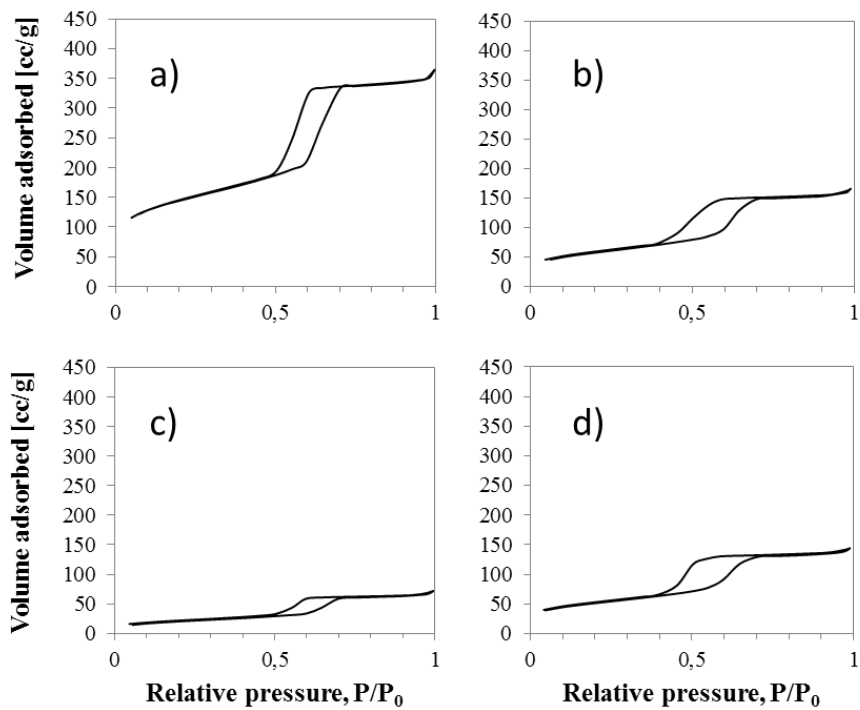


Figure 4.20 Nitrogen adsorption-desorption for a)COK-12_500, b)S_Alq_OMS(500)_4%_CaCl2, c)S_Alq_OMS(500)_8%_N2, d)S_Alq30_OMS70(500)_8%_CaCl2.

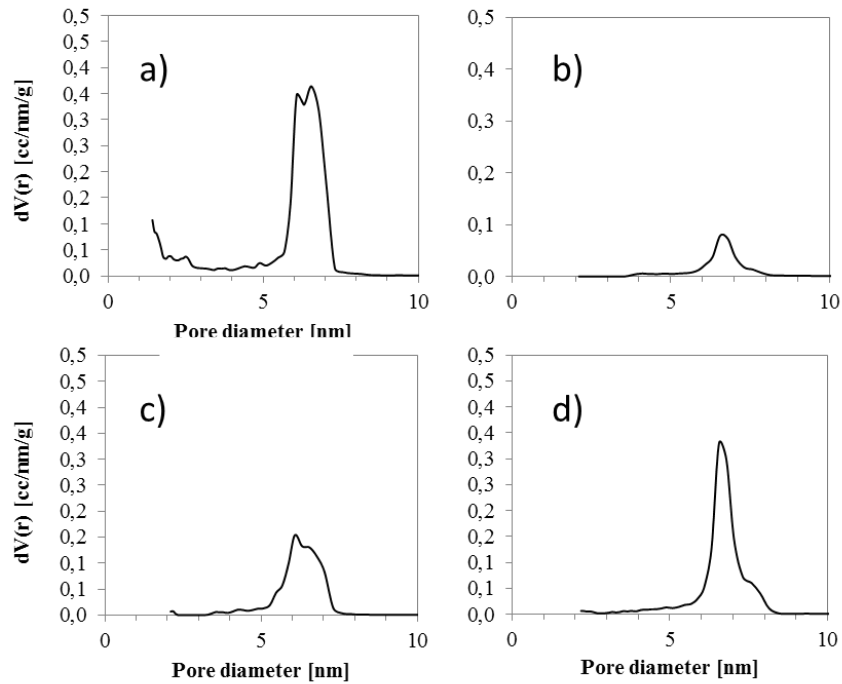


Figure 4.21 Pore size distribution of a)COK-12_400, b)S_AlgeOMS(400)_4%_CaCl₂, c)S_AlgeOMS(400)_8%_N₂, d)S_Alge30_OMS70(400)_8%_CaCl₂ as determined by the NLDFT method.

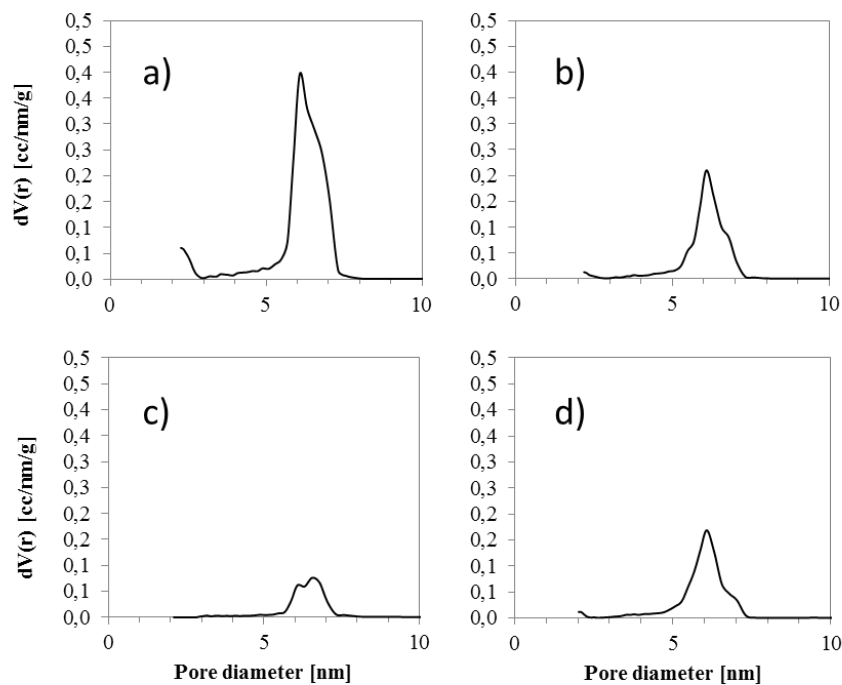


Figure 4.22 Pore size distribution of a)COK-12_400, b)S_AlgeOMS(500)_4%_CaCl₂, c)S_AlgeOMS(500)_8%_N₂, d)S_Alge30_OMS70(500)_8%_CaCl₂ as determined by the NLDFT method.

EDX measurements were done to see the chemical elements in the spheres. In the spheres S_Alge_ 8% it can be observed that there is an equal distribution. It can be seen in Figure 4.23 (right), where the chlorine atoms are distributed all over the picture. Observing the extracted spectrum (Figure 4.24), there is a little amount of silica is present, but if a look is taken on Figure 4.23 (down), it can be seen that it is only present in two concrete and small places. The reason for it could be that the hose used to produce the spheres was not completely clean from another previous use with a compound which contained silica.

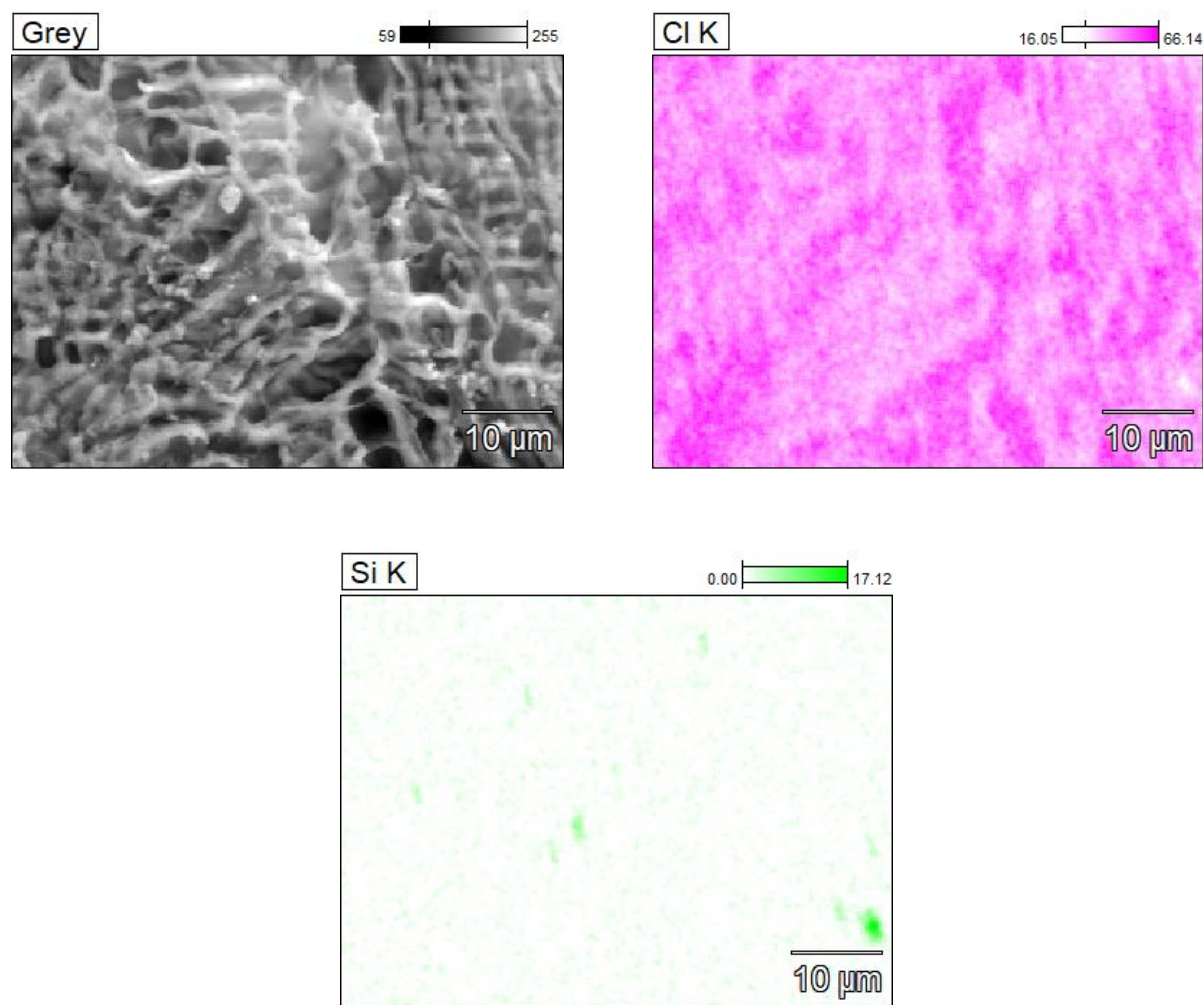


Figure 4.23 EDX S_Alge_ 8% (left), chlorine content (right) and silica content (down).

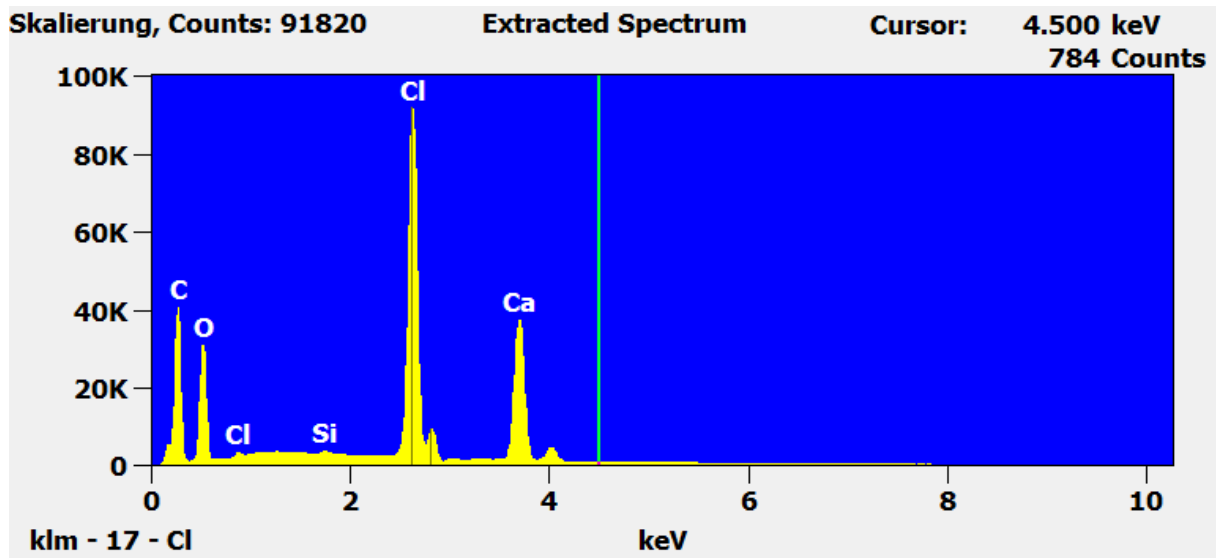


Figure 4.24 EDX S_Alge_8% extracted spectrum.

Taking a look on the extracted spectrum of the spheres S_Alge_OMS(500)_8%, a much higher amount of silica compared to the S_Alge_8% can be observed. It makes sense, because the silica is a proof for the OMS. OMS is not equally distributed all over the sample, there silica over the most parts of it, but in some parts the silica content is higher (Figure 4.25 (right)).

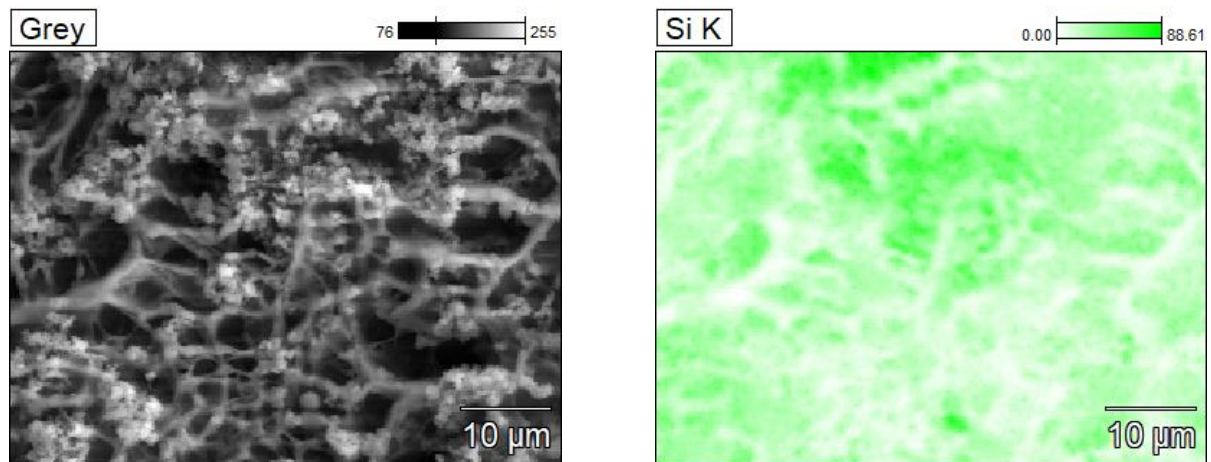


Figure 4.25 EDX S_Alge_OMS(500)_8% (left) and silica content (right).

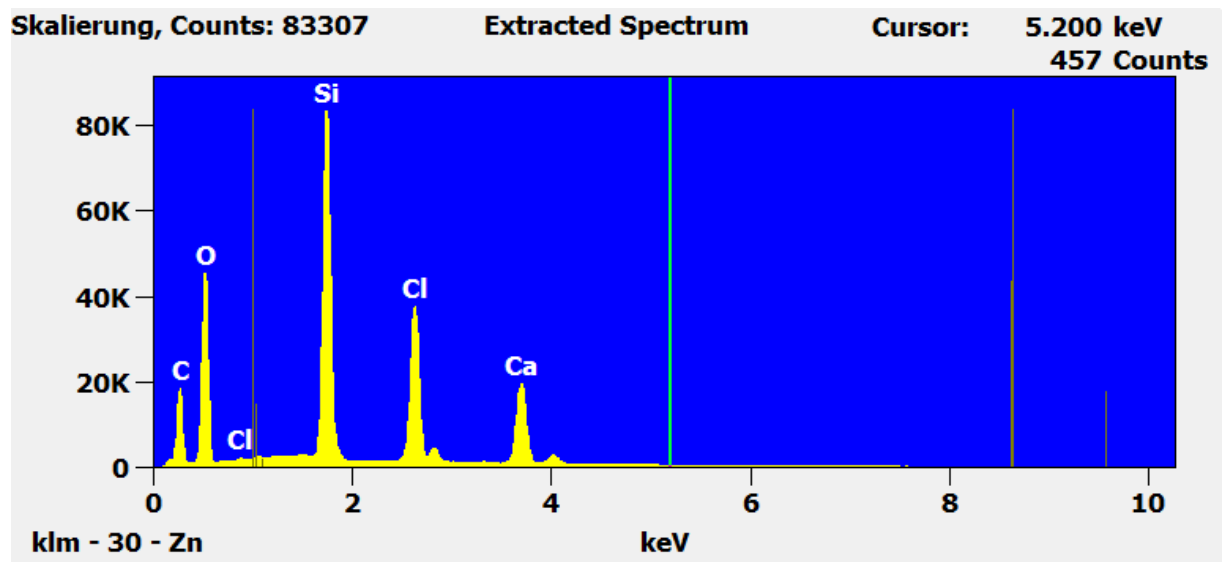


Figure 4.26 EDX S_Alg_OMS(500)_8% extracted spectrum.

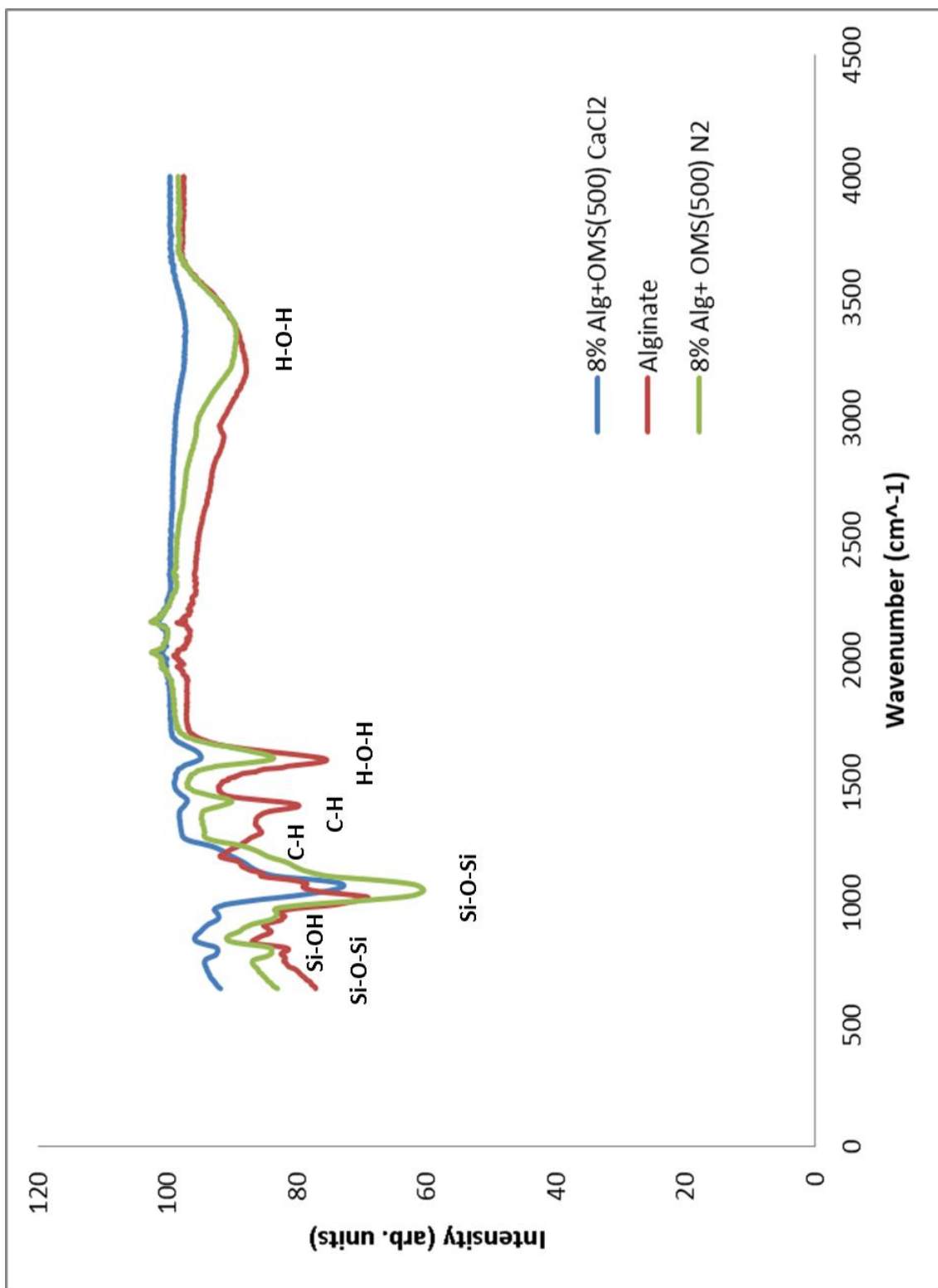


Figure 4.27 ATR-IR graph for Alginate, Alginate spheres, S_Alge_OMS(500)_8%_CaCl₂, S_Alge_OMS(500)_8%_N₂.

4.3.2 Solubility test

The results of the solubility test, obtained by ICP-Spectroscopy, can be seen in Table 4.6. It can be concluded that in the solutions with spheres produced with liquid nitrogen the calcium and silicon dissolved amount was significantly less compared to the solutions with the spheres produced without liquid nitrogen.

Observing the silicon amounts dissolved for the different solutions it doesn't make sense that in the solutions with spheres without OMS there is silicon. The amount is much less than in the solutions with spheres with OMS, but it shouldn't be any silicon dissolved. Maybe it is due to the fact that the same hose was used for all spheres production, although it was cleaned always after each use, or it could be also due to a measurement error.

Table 4.6 Mass of sodium, silica and calcium in water after a defined period of time with different spheres inside (solubility test). It was obtained by ICP-Spectroscopy.

Compound	Time in H ₂ O (h)	Na (mg/l)	Si (mg/l)	Ca (mg/l)
S_Alq_OMS(500)_8%_CaCl ₂	48	11.35	52.67	2.88
S_Alq_OMS(500)_8%_N ₂	48	3.38	47.92	1.03
S_Alq_OMS(500)_8%_CaCl ₂	96	18.35	24.13	2.01
S_Alq_OMS(500)_8%_N ₂	96	5.30	49.53	1.06
S_Alq_8%_CaCl ₂	96	13.88	6.44	2.54
S_Alq_8%_N ₂	96	9.41	1.89	2.27

4.3.3 Water purification test

Looking at the samples of the different solutions after being in contact with the adsorbants, some color differences can be observed. (Figure 4.28)

COK-12_500 worked with high removal efficiency for methylene blue (95.09%) and for rhodamine 6G (99.40%). Their adsorption capacity where 19.0 and 19.9 mg/g respectively. It can be noticed in the pictures of the samples, where the solutions in contact with COK-12_500 (1 B; 2 B) are much lighter than the initial solutions (1 A; 2 A). For congo red, COK-12_500 did not work, which can be observed in Figure 4.28 (3 B).

S_Alq_OMS(500)_8%_N₂ worked with high removal efficiency for methylene blue (92.41%) with an adsorption capacity of 18.5 mg/g. Although in the Figure 4.28 (1 C) the color of the sample is not as high as the sample with COK-12_500 (1 B), the UV analysis shows that it works. For congo red it apparently worked quite good (removal efficiency of 82% and adsorption capacity of 8.2 mg/g), but an experimental error was made: half of the volumen of initial congo red solution was put in comparison with the other 8 samples, but the mass of adsorbant was the same as in the other samples. For rhodamine 6G it did not work (removal efficiency of 4.58%), which can be observed in Figure 4.28 (2 C).

S_Algs_OMS(500)_8%_CaCl₂ worked with high removal efficiency for methylene blue (90.82%) with an adsorption capacity of 18.2 mg/g. For congo red it worked but with a lower removal efficiency (72.38%) and an adsorption capacity of 14.5 mg/g. It can be observed in Figure 4.28 where the sample with S_Algs_OMS(500)_8%_CaCl₂ (3 D) has a higher color than the original congo red solution (3 A). For rhodamine 6G it did not work (removal efficiency of 2.99%).

In contrast to rhodamine 6G, the OMS spheres show better removal efficiency (>72%) and an adsorption capacity of 8.2 mg/g for S_Algs_OMS(500)_8%_N₂ using a dosage of 10 g/l and 14.5 mg/g for S_Algs_OMS(500)_8%_CaCl₂ using a dosage of 5 mg/l. The main reason is that rhodamine 6G have a positive charge when it is in a water solution and the OMS powder has a negative charge, so that there is an attraction. Congo red has a negative charge when it is in a water solution, so there is repulsion between the OMS powder and the congo red. The spheres contain sodium alginate and they have a positive charge, so in this case there is an attraction between the congo red and the OMS spheres. Between the spheres and the rhodamine 6G there is a repulsion, because both have a positive charge. This would mean that it follows the model of the langmuir isotherm, but the spheres show also a high removal efficiency with methylene blue although both have a positive charge, so maybe there is another model which explains it better than the langmuir isotherm.

A positive aspect of the spheres in contrast to the powder is that they can be removed easier from the water.

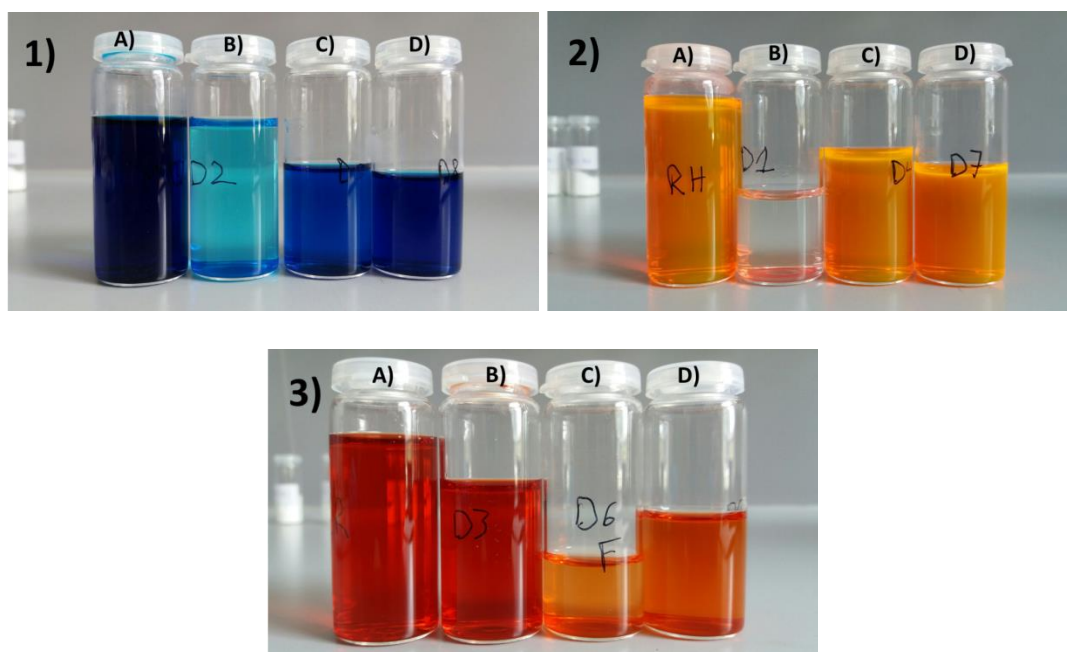


Figure 4.28 Samples of the different solutions: methylene blue (1), rhodamine 6G (2) and congo red (3) without adsorbant (A), with COK-12_500 (B), S_Algs_OMS(500)_8%_N₂ (C), S_Algs_OMS(500)_8%_CaCl₂.

Table 4.7 Adsorbance (mg/ml) and concentration (ppm) of each adsorbant for each solution.

Component	Adsorbant	Adsorbance (mg/ml)	Concentration (ppm)
MB	-	-	100
MB	COK-12_500	0.30	4.91
MB	S_Alge_OMS(500)_8%_N ₂	0.48	7.59
MB	S_Alge_OMS(500)_8%_CaCl ₂	0.58	9.18
RH	-	3.34	100
RH	COK-12_500	0.02	0.60
RH	S_Alge_OMS(500)_8%_N ₂	3.19	95.51
RH	S_Alge_OMS(500)_8%_CaCl ₂	3.24	97.01
CR	-	1.65	93.28
CR	COK-12_500	1.57	88.7
CR	S_Alge_OMS(500)_8%_N ₂	0.20	11.30
CR	S_Alge_OMS(500)_8%_CaCl ₂	0.37	20.90

MB: Methylene blue

RH: Rhodamine 6G

CR: Congo red

Table 4.8 Removal efficiency (%) and adsorption capacity (mg/g) of each adsorbant for each solution.

Component	Adsorbant	Removal efficiency (%)	Adsorption capacity (mg/g)
MB	COK-12_500	95.09	19.0
MB	S_Alge_OMS(500)_8%_N ₂	92.41	18.5
MB	S_Alge_OMS(500)_8%_CaCl ₂	90.82	18.2
RH	COK-12_500	99.40	19.9
RH	S_Alge_OMS(500)_8%_N ₂	4.49	0.9
RH	S_Alge_OMS(500)_8%_CaCl ₂	2.99	0.6
CR	COK-12_500	4.58	0.9
CR	S_Alge_OMS(500)_8%_N ₂	82.00	8.2
CR	S_Alge_OMS(500)_8%_CaCl ₂	72.38	14.5

MB: Methylene blue

RH: Rhodamine 6G

CR: Congo red

4.4 Tape production

A very thin and flexible membrane was obtained, as it can be seen in Figure 4.29 and Figure 4.30. For the ones with alginate in its composition it didn't work at the beginning, as it can be observed in Figure 4.31 and Figure 4.32, because the membranes got destroyed in the freeze drying process. But finally, by increasing the thickness of the membrane from 0.2 mm to 0.5 mm it worked for a composition of T_Alg95_OMS5(400)_8%.



Figure 4.29 Tapes compound of alginate: T_Alg_4% (LEFT) and T_Alg_8% (RIGHT).

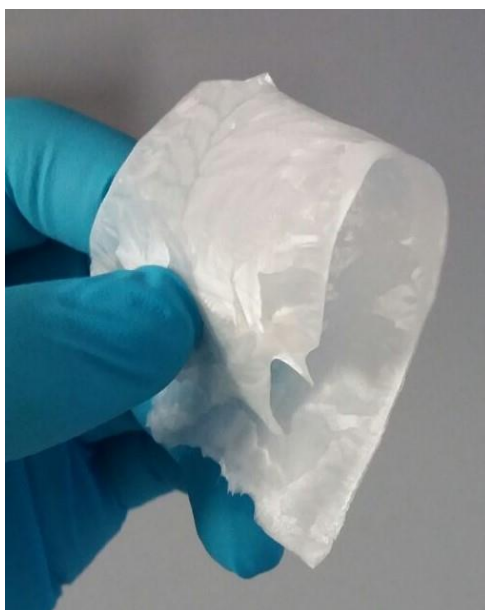


Figure 4.30 Tape compound of alginate 8 wt%.

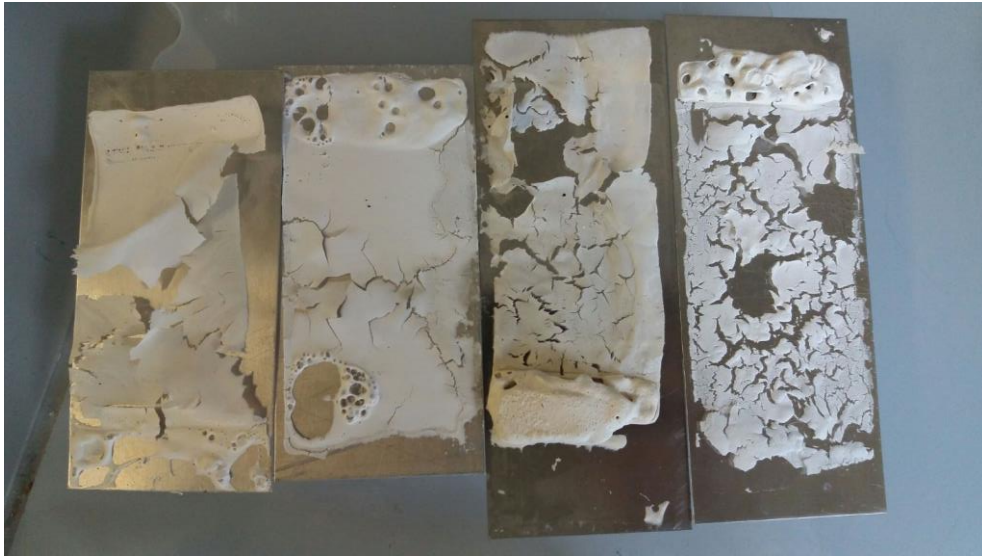


Figure 4.31 Tapes compound of alginate and COK-12 with different compositions: A) T_Alg60_OMS40(400)_8%, B) T_Alg_OMS(400)_8%, C) T_Alg70_OMS30(400)_8%, D) T_Alg_OMS(400)_8%.



Figure 4.32 Tapes compound of alginate and COK-12 with different compositions: A) T_Alg90_OMS10(400)_8%, B) T_Alg95_OMS5(400)_8%.

REM pictures were taken to observe the structure of the membranes. In Figure 4.33 it can be observed that the membrane with a composition of 4 wt% alginate is full of pores of different sizes. The membrane with a composition of 8 wt% alginate has much more pores than the membrane just mentioned, which can be seen in Figure 4.34.

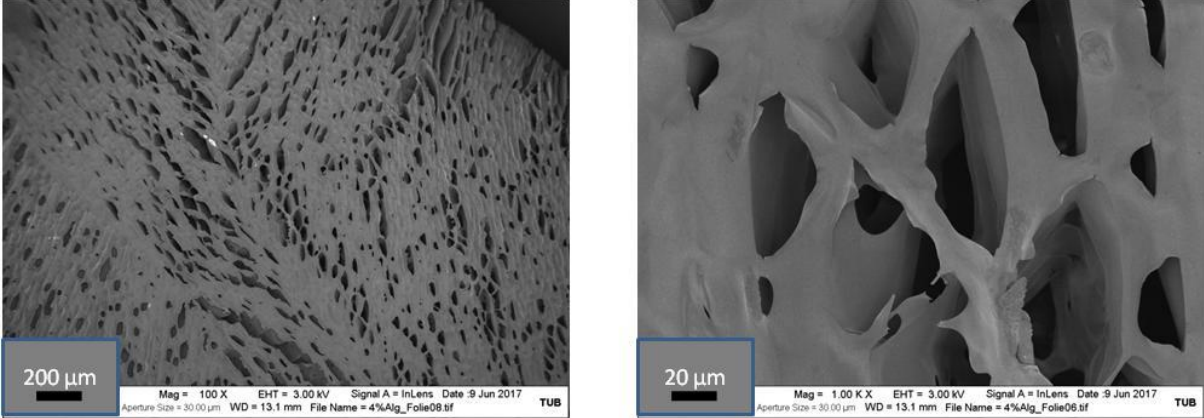


Figure 4.33 SEM-images of Alginate [4%] film transversal section.

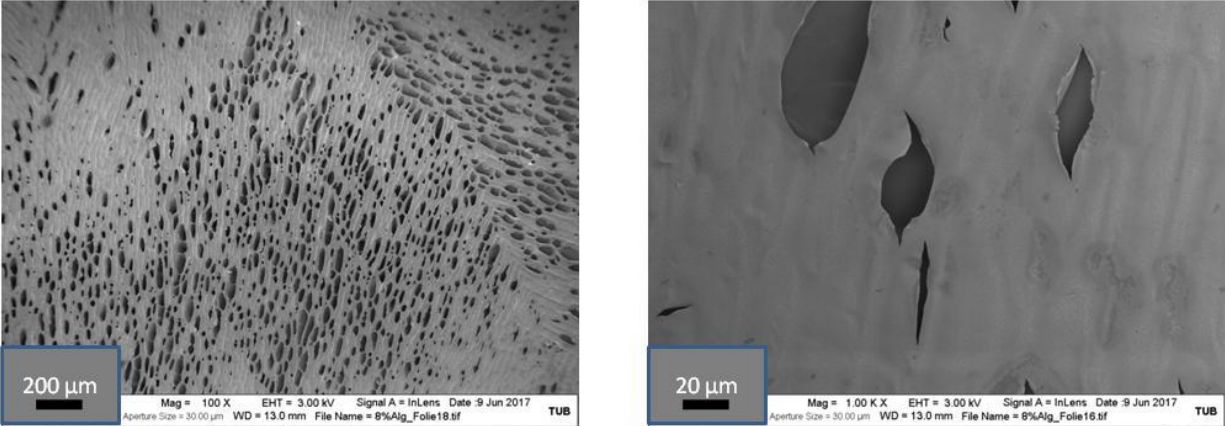


Figure 4.34 SEM-images of Alginate [8%] film transversal section.

In Figure 4.35 the cross section of the membrane T_Al95_OMS5(400)_8% can be seen. It can be observed that the pores go from one side to the other and that there are also pores in the transversal direction.

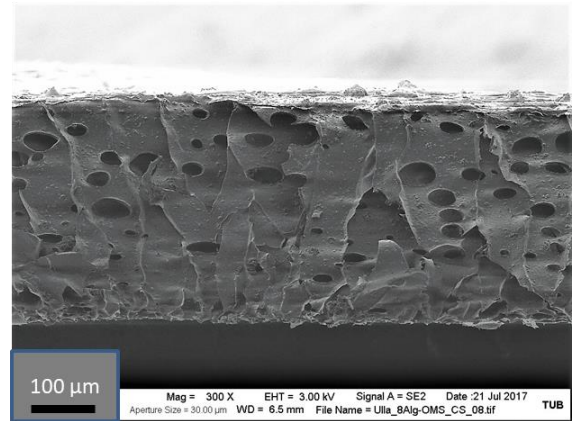
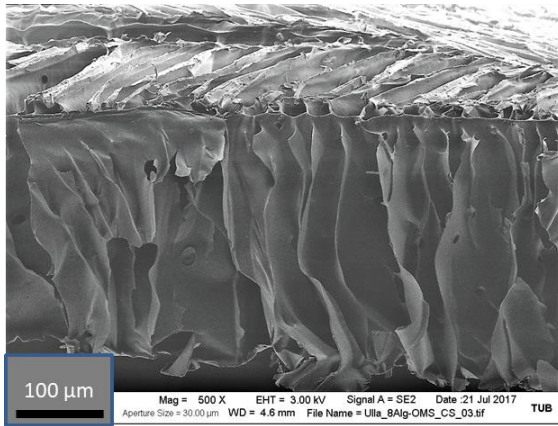


Figure 4.35 REM T_Alg95_OMS5(400)_8% cross section.

In Figure 4.36 the transversal section of the membrane mentioned above can be observed. There are many pores of different sizes and looking on the close área, the OMS can be observed inside of the alginate.

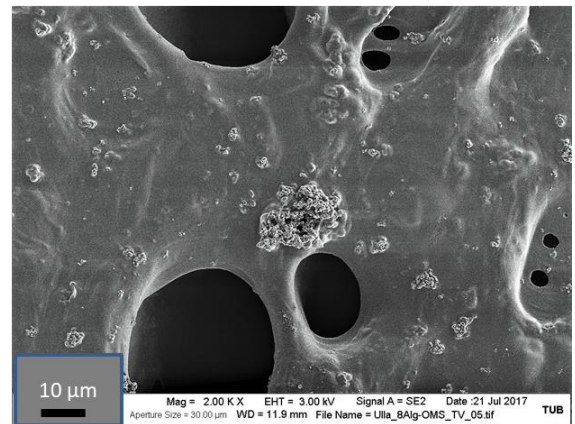
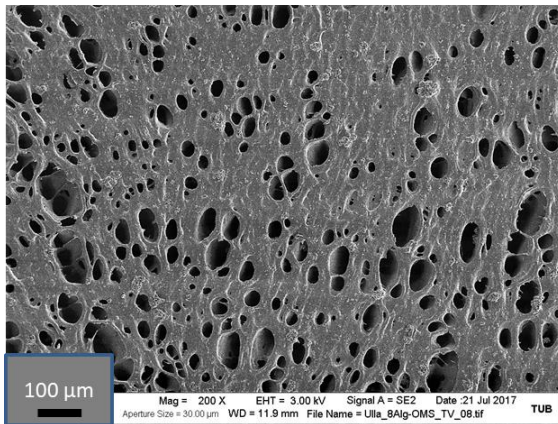


Figure 4.36 REM T_Alg95_OMS5(400)_8% transversal section.

5 Conclusions and outlook

The first goal of this work, which was to produce COK-12 in large quantities, maintaining its characteristic mesostructure, was accomplished successfully. The OMS material exhibits the expected mesostructured for materials templated with the triblock copolymer P123. A bigger amount of the material in comparison with others reported before was synthesized in batch.

Different calcination temperatures ranging from 350°C to 900°C were studied to see how the final product changes. The calcination temperature at the removal of the template had an important influence on the material characteristics. Apart from the color of the material, which is brown at low calcination temperatures and white at calcination temperatures higher than 450 °C, it was observed that the pore size of the COK-12 decreases with the calcination temperature. Another fact that was confirmed by SAXRD experiments is that the long-range hexagonally ordering is higher at lower temperatures. But one of the most important facts discovered is that the amount of silanol groups decreases with the calcination temperatures. There is a need of silanol groups for further surface functionalization of COK-12 with functional organic groups, which could be relevant for example for medical applications, sorption or drug delivery. Carbon groups could be also important for further functionalization and they decrease with the calcination temperature. Therefore, depending on the groups needed for the functionalization the calcination should be done at higher or lower temperatures.

A second method to remove the template from the material was studied, the extraction with methanol, but it didn't work as expected. Different periods inside of the ultrasonicator were tested, but in all of them the carbon content after the extraction was very high. It is possible, that increasing the temperature in the ultrasonicator and using longer periods it works better. This could be studied in the future, because the extraction has some important benefits in comparison to the calcination: it would be cheaper, faster, with less environmental impact and it could have positive effect on surface characteristics

The third goal of this work was to produce spheres composing of alginate and COK-12. After trying two different methods, production with liquid nitrogen and without liquid nitrogen, the results of the analysis showed that spheres produced with liquid nitrogen had much more and bigger pores, which could be a positive aspect for some applications. In the spheres produced with liquid nitrogen there are more silanol groups, which is also an important reason to use these spheres in stead of the spheres produced without liquid nitrogen.

The fourth goal, producing membranes or films compound of alginate and COK-12, was carried out successfully, although only membranes with a little percentage of COK-12 were obtained. The membranes produced are very thin and flexible. Pores in the cross and transversal direction were observed in REM pictures, which is a positive aspect for the use of these membranes in application fields such as catalysis. A continuous or semi-continuous membrane production could be possible due to the fact, that the freezing process takes place in less than 1 minute with the process employed for this work.

6 References

1. J. Jammaer, A. Aerts, J. D'Haen, J. W. Seo, and J. A. Martens: 'Convenient synthesis of ordered mesoporous silica at room temperature and quasi-neutral pH', *J. Mater. Chem.*, 2009, 19(44), 8290, doi: 10.1039/b915273c.
2. K. S. W. Sing, D. H. Everett, R. A. W. Haul, L. Moscou, R. A. Pierotti, J. Rouquerol, and T. Siemieniewska: 'Reporting physisorption data for gas/solid systems: with special reference to the determination of surface area and porosity', *Pure & Appl. Chem.*, 57(4), 603–619.
3. M. Manzano and M. Vallet-Regi: 'New developments in ordered mesoporous materials for drug delivery', *J. Mater. Chem.*, 2010, 20(27), 5593, doi: 10.1039/b922651f.
4. A. Walcarius: 'Mesoporous materials and electrochemistry', *Chem. Soc. Rev.*, 2013, 42(9), 4098, doi: 10.1039/c2cs35322a.
5. T. Wagner, S. Haffer, C. Weinberger, D. Klaus, and M. Tiemann: 'Mesoporous materials as gas sensors', *Chem. Soc. Rev.*, 2013, 42(9), 4036–4053, doi: 10.1039/C2CS35379B.
6. M. Hartmann: 'Ordered Mesoporous Materials for Bioadsorption and Biocatalysis', *Chem. Mater.*, 2005, 17(18), 4577–4593, doi: 10.1021/cm0485658.
7. T.-L. Chew, A. L. Ahmad, and S. Bhatia: 'Ordered mesoporous silica (OMS) as an adsorbent and membrane for separation of carbon dioxide (CO₂)', *Advances in Colloid and Interface Science*, 2010, 153(1-2), 43–57, doi: 10.1016/j.cis.2009.12.001.
8. K. Moller and T. Bein: 'Inclusion Chemistry in Periodic Mesoporous Hosts', *Chem. Mater.*, 1998, 10(10), 2950–2963, doi: 10.1021/cm980243e.
9. A. Monnier, F. Schuth, Q. Huo, D. Kumar, D. Margolese, R. S. Maxwell, G. D. Stucky, M. Krishnamurty, P. Petroff, A. Firouzi, M. Janicke, and B. F. Chmelka: 'Cooperative Formation of Inorganic-Organic Interfaces in the Synthesis of Silicate Mesostructures', *Science*, 1993, 261(5126), 1299–1303, doi:10.1126/science.261.5126.1299.
10. R. Takahashi, K. Nakanishi, and N. Soga: 'Aggregation Behavior of Alkoxide-Derived Silica in Sol-Gel Process in Presence of Poly(ethylene oxide)', *Journal of Sol-Gel Science and Technology*, 2000, 17(1), 7–18, doi: 10.1023/A:1008753718586.
11. J. Jammaer, T. S. van Erp, A. Aerts, C. E. A. Kirschhock, and J. A. Martens: 'Continuous Synthesis Process of Hexagonal Nanoplates of P 6 m Ordered Mesoporous Silica', *J. Am. Chem. Soc.*, 2011, 133(34), 13737–13745, doi: 10.1021/ja205627t.
12. G. Q. Lu and X. S. Zhao: 'Nanoporous materials: Science and engineering / edited by G.Q. Lu, X.S. Zhao'; 2004, London, Imperial College Press.
13. J. Jammaer, A. Aerts, J. D'Haen, J. W. Seo, and J. A. Martens: 'Convenient synthesis of ordered mesoporous silica at room temperature and quasi-neutral pH', *J. Mater. Chem.*, 2009, 19(44), 8290, doi: 10.1039/b915273c.

14. H. Minakuchi, K. Nakanishi, N. Soga, N. Ishizuka, and N. Tanaka: 'Octadecylsilylated porous silica rods as separation media for reversed-phase liquid chromatography', *Analytical chemistry*, 1996, 68(19), 3498–3501, doi: 10.1021/ac960281m.
15. A. Sachse, A. Galarneau, F. Fajula, F. Di Renzo, P. Creux, and B. Coq: 'Functional silica monoliths with hierarchical uniform porosity as continuous flow catalytic reactors', *Microporous and Mesoporous Materials*, 2011, 140(1-3), 58–68, doi: 10.1016/j.micromeso.2010.10.044.
16. J. Jammaer, A. Aerts, J. D'Haen, J. W. Seo, and J. A. Martens: 'Convenient synthesis of ordered mesoporous silica at room temperature and quasi-neutral pH', *J. Mater. Chem.*, 2009, 19(44), 8290, doi: 10.1039/b915273c.
17. L. T. Gibson, Mesosilica materials and organic pollutant adsorption: part A removal from air. <http://pubs.rsc.org/en/content/articlelanding/2014/cs/c3cs60096c/unauth#ldivAbstract>
18. BIOSAXS GmbH, Small angle X-ray scatterings. <http://biosaxs.com/technique.html>
19. TAP (Teaching Advanced Physics), Episode 530: X-ray diffraction. http://tap.iop.org/atoms/xray/530/page_47297.html
20. G. Q. Lu and X. S. Zhao: 'Nanoporous materials: Science and engineering / edited by G.Q. Lu, X.S. Zhao'; 2004, London, Imperial College Press.
21. John P Jasper; Benjamin J Westenberger; J.A. Spencer; Moheb Nasr, Stable isotopic characterization of active pharmaceutical ingredients. https://www.researchgate.net/publication/8670231_Stable_isotopic_characterization_of_active_pharmaceutical_ingredients

List of figures

Figure 1.1 Illustrative cross-section of a porous solid. For details see Table 1.1.....	2
Figure 1.2 True liquid crystal templating mechanism (a) and the cooperative self-assembly mechanism (b) for production of MCM-41.	3
Figure 1.3 Schematic representation of the stages of formation of COK-12. (a) Silica species precipitate on the PEO blocks of the spherical P123 micelles which are in solution. (b) At a critical silica concentration, steric stabilization is lifted and (c,d) spherical micelles coalesce into cylinders that increase in size. (e) Further addition of silica species leads to the aggregation of the cylinders and eventually to the formation of a 2-dimensional hexagonally ordered mesostructure ²⁰⁹	5
Figure 2.1 Schematic representation of the functioning of SAXS.	7
Figure 2.2 Bragg's law of diffraction, in which three radiation waves of identical wavelength interact with three atoms within crystalline solid and are scattered.	7
Figure 2.3 Types of adsorption isotherms as classified by IUPAC. See text for details.	8
Figure 2.4 Schematic representation of multilayer adsorption, pore condensation and hysteresis in a single pore. (A) monolayer formation, (B) multilayer adsorption, (C-D) capillary condensation, (E) pore evaporation by a receding meniscus, (F) desorption.	9
Figure 2.5 Types of hysteresis	10
Figure 2.6 Schematic representation of the functioning of elemental analysis.....	13
Figure 3.1 Immediately solid formation just after adding the silicate solution (left) and filtration process (right).	15
Figure 3.2 Solids after filtration.....	15
Figure 3.3 Schematic of COK-12 batch production with two different methods to remove the organic templating agent: calcination and extraction.	17
Figure 3.4 Spheres production with liquid nitrogen.	18
Figure 3.5 Spheres production with calcium chloride.	19
Figure 3.6 Schematic of spheres production with two different methods: with calcium chloride and with liquid nitrogen.	20
Figure 3.7 Solutions of methylene blue, rhodamine 6G and congo red stirred with different adsorbants: COK-12_500, S_Alge_OMS(500)_8%_N2, S_Alge_OMS(500)_8%_CaCl2.	21
Figure 3.8 Films production with liquid nitrogen inside of the metal box.	22
Figure 3.9 Schematic of films production.	23
Figure 4.1 Comparison of COK-12 obtained with methanol extraction (left) and calcination at 350 °C, 400°C, 450 °C and 500 °C.	25
Figure 4.2 TEM micrographs of COK-12 calcined at 350°C.	26
Figure 4.3 TEM micrographs of COK-12 calcined at 400°C.	26
Figure 4.4 TEM micrographs of COK-12 calcined at 450°C.	27
Figure 4.5 TEM micrographs of COK-12 calcined at 700°C.	27
Figure 4.6 Nitrogen adsorption-desorption for COK-12 calcined at different temperatures from 350°C to 900°C and 2 extractions with methanol. The isotherms are all type IV with H1 hysteresis (apart from the higher temperatures, from 700°C up to 900°C), characteristic of mesoporous materials.....	28
Figure 4.7 Pore size distribution of COK-12 calcined at different temperatures from 350°C to 900°C and 2 extractions with methanol as determined by the NLDFT method.	30
Figure 4.8 SAXRD patterns of COK-12 calcined at different temperatures from 350°C to 900°C and 2 extractions with methanol.	32
Figure 4.9 ATR-IR graph for COK-12 uncalcined and calcined at 350 °C, 400 °C, 500°C, 650°C and 900 °C.....	34
Figure 4.10 ATR-IR graph for COK-12 uncalcined, calcined at 500 °C and COK-12 produced with 10 min and 2x5 min methanol extraction.	37

Figure 4.11 Comparison of COK-12 calcined at 400 °C (A), S_Al70_OMS30(400)_8%_CaCl2 and S_Al70_OMS30(400)_8%_N2.....	38
Figure 4.12 Pictures of all spheres done for this thesis. The sample codes can be read on Table 4.3.	39
Figure 4.13 REM S_Al70_OMS30(400)_8%_N2.....	41
Figure 4.14 REM S_Al70_OMS30(400)_8%_CaCl2.....	41
Figure 4.15 REM S_Al70_OMS30(400)_4%_CaCl2.....	42
Figure 4.16 REM S_Al70_OMS30(400)_8%_CaCl2.....	42
Figure 4.17 REM S_Al70_OMS30(400)_8%_CaCl2.....	43
Figure 4.18 REM S_Al70_OMS30(400)_8%_N2.....	43
Figure 4.19 Nitrogen adsorption-desorption for a)COK-12_400, b)S_Al70_OMS30(400)_4%_CaCl2, c)S_Al70_OMS30(400)_8%_N2, d)S_Al70_OMS30(400)_8%_CaCl2.....	46
Figure 4.20 Nitrogen adsorption-desorption for a)COK-12_500, b)S_Al70_OMS30(400)_4%_CaCl2, c)S_Al70_OMS30(400)_8%_N2, d)S_Al70_OMS30(400)_8%_CaCl2.....	46
Figure 4.21 Pore size distribution of a)COK-12_400, b)S_Al70_OMS30(400)_4%_CaCl2, c)S_Al70_OMS30(400)_8%_N2, d)S_Al70_OMS30(400)_8%_CaCl2 as determined by the NLDFT method.....	47
Figure 4.22 Pore size distribution of a)COK-12_400, b)S_Al70_OMS30(400)_4%_CaCl2, c)S_Al70_OMS30(400)_8%_N2, d)S_Al70_OMS30(400)_8%_CaCl2 as determined by the NLDFT method.....	47
Figure 4.23 EDX S_Al70_OMS30(400)_8% (left), chlorine content (right) and silica content (down).....	48
Figure 4.24 EDX S_Al70_OMS30(400)_8% extracted spectrum.....	49
Figure 4.25 EDX S_Al70_OMS30(400)_8% (left) and silica content (right).....	49
Figure 4.26 EDX S_Al70_OMS30(400)_8% extracted spectrum.....	50
Figure 4.27 ATR-IR graph for Alginate, Alginate spheres, S_Al70_OMS30(400)_8%_CaCl2, S_Al70_OMS30(400)_8%_N2.....	51
Figure 4.28 Adsorbance (mg/ml) and concentration (ppm) of each solution after 2 h stirred with the adsorbants.....	53
Figure 4.29 Tapes compound of alginate: T_Al70_OMS30(400)_4% (LEFT) and T_Al70_OMS30(400)_8% (RIGHT).....	55
Figure 4.30 Tape compound of alginate 8 wt%.....	55
Figure 4.31 Tapes compound of alginate and COK-12 with different compositions: A) T_Al70_OMS30(400)_8%, B) T_Al70_OMS30(400)_8%, C) T_Al70_OMS30(400)_8%.....	56
Figure 4.32 Tapes compound of alginate and COK-12 with different compositions: A) T_Al70_OMS30(400)_8%, B) T_Al70_OMS30(400)_8%.....	56
Figure 4.33 SEM-images of Alginate [4%] film transversal section.....	57
Figure 4.34 SEM-images of Alginate [8%] film transversal section.....	57
Figure 4.35 REM T_Al70_OMS30(400)_8% cross section.....	58
Figure 4.36 REM T_Al70_OMS30(400)_8% transversal section.....	58

List of tables

Table 1.1 Classification of pores according to the IUPAC.	1
Table 3.1 Synthesis conditions for upscaled COK-12 materials synthesis.....	16
Table 3.2 Calcination temperatures used and times in the ultrasonicator used for the methanol extraction.	16
Table 3.3 List of the different spheres produced with its compositions. Each type of spheres was done twice: one time only with calcium chloride (CaCl ₂) and one time also with liquid nitrogen (N ₂).	19
Table 3.4 List of the different films produced with its compositions.	23
Table 4.1 Nitrogen, carbon, hydrogen, sulfur, silicon and sodium content of COK-12uncalcined, calcined at different temperatures from 350°C to 900°C and 2 extractions with methanol.	25
Table 4.2 Surface area, pore width, pore volume and micropore volume of COK-12 calcined at different temperatures from 350°C to 900°C and 2 extractions with methanol.	31
Table 4.3 Sample codes according to the number of the spheres shown in Figure 4.X.....	40
Table 4.4 Surface area, pore width, pore volume and micropore volume of spheres with COK-12 calcined at 400 °C.	44
Table 4.5 Surface area, pore width, pore volume and micropore volume of spheres with COK-12 calcined at 500 °C.	45
Table 4.6 Mass of sodium, silica and calcium in water after a defined period of time with different spheres inside (solubility test). It was obtained by ICP-Spectroscopy.	52
Table 4.7 Adsorbance (mg/ml) and concentration (ppm) of each adsorbant for each solution.....	54
Table 4.8 Removal efficiency (%) and adsorption capacity (mg/g) of each adsorbant for each solution.	54